Modelling of Condensed Mode Cooling during the Polymerization of Ethylene in Fluidized Bed

Rita Ferreira Alves, Timothy Mckenna

Modelling of Condensed Mode Cooling during the Polymerization of Ethylene in Fluidized Bed Reactors

Rita Ferreira Alves, Timothy F.L. McKenna*

Catalyse, Polymérisation, Procédés et Matériaux UMR-5128, Université de Lyon, CNRS, CPE-Lyon, UCB Lyon-1, 43 Blvd du 11 Novembre 1918, 69616 Villeurbanne Cedex, France

*timothy.mckenna@univ-lyon1.fr

Abstract

A reactor model for the gas-phase production of ethylene has been developed to investigate the effects of condensed mode operation, i.e., reactor operation in the presence of an induced condensing agent (ICA). The ICA not only improves heat evacuation from the reactor, but it also has a thermodynamic effect on the ternary system ethylene/ICA/polymer (such as co-solubility and co-diffusion), which are often overlooked. The proposed model is based on the compartmentalization of a fluidized bed reactor into a series of interconnecting CSTR tanks. It includes three major lengths-scales: micro-scale (polymerization kinetics, molecular weight distributions), meso-scale (ternary thermodynamic model, single particle model, droplet evaporation) and macro-scale modelling (populations balance equations). A criteria for defining compartment height based on the modelling objectives of this work is also proposed and the effects of number/height of compartments in the model predictions are studied. The model is validated with patent data and shows good agreement with two sets of data from different sources. The effects of two ICA (n-pentane or n-hexane) are studied and the results show that increased ICA liquid content leads to less steep temperature profiles and increased production rates. The effects of other operating conditions such as hydrogen content, operating temperature,

liquid droplet size, polymer recovery height and liquid injection height are studied. They all showed good agreement with the available experimental results found in the literature. A scale-down exercise was also carried out where industrial and pilot scale reactors are compared.

1 Introduction

Polyethylene is the most widely produced thermoplastic in the world. The reactors for its production have obviously been the target of multiple modelling [1]–[4]. Industrial processes for PE production in gas-phase predominately use one or more fluidized bed reactors (FBR, seeFigure 1), where a feed stream containing ethylene, hydrogen and other monomers, along with inert gases, is fed at the bottom of the reactor through a distribution plate (and occasionally through nozzles placed inside the lower portion of the reactor). The catalyst (or prepolymerized) particles are fed to reactor just above this plate, where they are contacted with the monomer(s) and a highly exothermic polymerization reaction takes place. The unreacted monomer(s), hydrogen and inerts are recovered at the top of the bed after a disengagement zone, which is meant to ensure that the gas does not carry solid particles into the recycle loop. The recycled vapors are purged, compressed, and cooled. Make-up monomer, hydrogen, and eventually other compounds are introduced before feeding this stream back into the reactor. The newly formed polymer is recovered at the bottom of the bed through one or more discharge valves, and is fed into a series of degassing tanks.

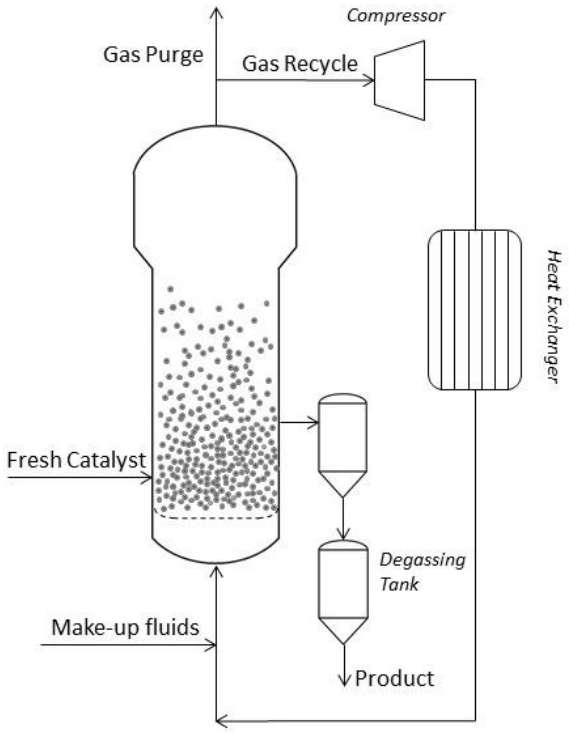

Figure 1. Schema of a typical polyethylene polymerization process.

Recent advances in catalyst technology have made it possible to produce several tens of kilograms of polymer per gram of supported catalyst. This, combined with the highly exothermic nature of the reaction means that heat evacuation can be a challenge, and the upper limit on polymer production rates (space-time yield) is often imposed by the amount of heat that can be removed from the reactor. It is widely thought that most of the heat generated in the polymerizing particles is removed by convective heat transfer between the particles and the gas phase as the latter rapidly flows through the bed of hot particles. To further enhance the heat removal, the inlet temperature of the gas can be lowered, but only to a certain point as large temperature gradients in the reactor should be avoided for reasons linked to polymer quality, and the fact that if the bed is too cold, the productivity will drop. Another means of improving heat transfer might be to manipulate the gas velocity, although this is not practical for reasons linked to the

fluidization of the particles. If the velocity is too high, the particles are pneumatically conveyed out of the bed which can cause problems downstream, and if it is too low, the bed will collapse. An alternative to these two solutions presents itself when the physical nature of the feed stream is altered. The heat capacity of the gas stream can be increased by adding inert alkanes, like propane or isomers of butane, pentane or hexane. If such compounds are added in the vapor phase, the reactor is working under *super-dry mode*. Even more heat can be removed if the reactor is operating under *condensed mode*, where a fraction of these inert compounds is condensed before being fed to the reactor. For this reason, the inert alkanes are known as *Induced Condensing Agents* (ICA). In condensed mode, the liquid is sprayed into the reactor in the form of small droplets. As soon as the liquid droplets reach a warm spot in the reactor they evaporate, thereby providing local cooling where it is needed. The portion of the bed containing a 3-phase mixture (gas, solid, liquid droplets) will depend on the inlet temperature, amount of liquid in the feed, and the dew point of the feed stream.

However, adding ICA has more consequences than simply improving the heat removal. It has been shown experimentally that adding an ICA has a measurable effect on the observed rate of polymerization [5]–[7]. It turns out that the well-known *co-solubility effect*, where the concentration of ethylene in the polymer amorphous phase is increased by the presence of a heavier hydrocarbons, can increase the rate of polymerization and the average molecular weights [5]–[9]. Furthermore, it has been shown that the presence of ICA in the amorphous polymer phase can also effect the mass diffusion in the polymer: as the ICA swells the polymer particles, it effectively increases the polymer free volume, which aids in the transport of monomer(s) from the particle surface to the active sites [8], [10]. While the following issues will not be discussed in this paper, it should be pointed out that the ICA also acts as a plasticizer, which is proven to

slow the crystallization rate [11]. Furthermore, a decrease in the melting point caused by the presence of ICA can cause particles to be stickier and therefore increase agglomeration in the reactor [11][12].

Given their commercial importance, gas phase polymerization processes have been the target of multiple modelling efforts. The advantages and disadvantages of these different approaches have been discussed in various review articles [1]–[4], [13], [14] which the reader is referred for a detailed discussion. The general conclusions we draw from these modelling studies are:

1. For certain applications the well mixed simplification (i.e. the powder phase of the FBR can be treated as an ideal continuous stirred tank reactor – CSTR) works well. For instance, it can capture the over impact of changing feed rates and compositions, or changes in the average reactor temperature on productivity and average polymer properties. It cannot be used to predict variations in temperature and composition in the bed.
2. Two phase models, which allow for the separate exist of bubble (gas) and emulsion (dense powder with the gas phase at the minimum fluidization velocity) can provide slightly more detail, in particular about heat transfer if one allows the bubble size to change as a function of bed height.
3. In order to capture more complex phenomena, more complex models are required. For instance, dividing emulsion and/or bubble phases up into compartments allows one to estimate temperature gradients in the reactor, and thus to obtain a more accurate picture of the evolution of polymerization rate and polymer properties, as well as phenomena such as bed segregation. In theory, the use of compartmentalized models will also allow one to include two- and three-phase regions in a reactor model.

4. The importance of including a separate bubble phase in the compartmentalized models is not obvious. There appears to be limited impact on the heat removal in the reactor, but this depends on a number of adjustable parameters, and eventually on the inclusion of a limited fraction of the powder phase in the bubbles themselves.
5. There are very few models that account for the impact of gaseous ICA, and even fewer for the presence of liquid ICA in the reactor. Mirzaei *et al* [15] employed the SL-EoS for the calculation of ethylene concentration at the active sites in a super dry FBR, but their thermodynamic model was only applied in a binary fashion, which left out the co-solubility effect. Others [16], [17] developed a compartmentalized model with a plug flow compartment at the bottom and one large CSTR-like compartment above it to account for liquid evaporation at the bottom of the reactor, but no thermodynamic model was used to include the impact of ICA. It appears that only Alves et al. [18] included the impact of adding an ICA during the homopolymerization of ethylene while accounting for the co-solubility effect. The simplified single phase CSTR approximation worked well in predicting the increase in productivity, and decrease in catalyst mileage due to the co-solubility effect [19]. However, the authors did not attempt to look at the impact of ICA on polymer properties, nor did they include a single particle model, temperature gradients in the bed or condensed mode operation.

In the current paper we have developed a model of a gas phase fluidized bed reactor to investigate the effects of ICA during ethylene polymerization in dry, super dry and condensed modes of operation. The model includes the compartmentalization of the bed, which allows to include temperature gradients in the reactor, coupled with a single particle model and a ternary thermodynamic model (SL-EoS) in order to describe the impact of ICA on solubility of ethylene

and on ethylene diffusion in the particles. Population balance equations (PBE) are included to account for the impact of particle size on the polymerization rate, bed segregation and on particle elutriation. Finally, a droplet evaporation model to account for the phase change of the ICA introduced to the reactor.

2 Model Development

As we wish to predict the distribution of liquid droplets in the reactor, and to understand the influence of ICA on the temperature profile of the bed, the reactor model will treat the FBR as a cascade of interconnected compartments, where each compartment is assumed to behave like an ideal continuous stirred tank reactor (CSTR). The compartments contain only the emulsion phase (particles and gas). The model does not account for heat and mass transfer between the emulsion phase and gas bubbles that most likely form in the FBR. As mentioned above and described by Alves et al. [1], a separate bubble phase as the uncertainty in terms of estimating bubble size, and mass and heat transfer between bubble and emulsion phase adds additional complexity to the model that is not warranted in terms of the understanding obtained from the model. As it will be shown below, treating the FBR as a cascade of "emulsion" CSTRs can adequately describe the dynamics of the polymerization in such a reactor. Finally, although compartmentalization has been used in previous studies (e.g. [20]–[22]), it seems that there has been no real discussion on how to determine the compartment size. Therefore, the developed model includes bed compartmentalization based on a well-defined criterion.

To model the FBR, we need:

1. A kinetic model to describe the rate of polymerization and polymer properties as a function of temperature and composition.

2. A thermodynamic model for diffusion and absorption of multicomponent mixtures in the polymer phase of the particle covering the active sites.
3. A model for transport of the sorbed species in the growing polymer particles to determine the concentration of monomer at the active sites, and ideally a heat transfer model to follow the particle temperature and the amount of heat released into the continuous phase of the reactor.
4. A population balance model to account for the impact of the particle size distribution and to estimate phenomena such as elutriation and bed segregation under different reactor conditions.
5. A model for droplet evaporation. In condensed mode cooling, portions of the reactor volume contain 3 phase mixtures of vapor, particles and evaporating liquid droplets. It is important to understand where the droplets are in the reactor as this will have an impact on the local temperature among other things.
6. A model for the residence time distribution of the particles in the reactor (e.g. the compartment model presented here).

The final point is the crux of the current paper, but it is necessary to discuss the first three points as they will have an important impact on how the reactor behaves.

2.1 Model Compartmentalization

In the present model the FBR is divided into *n* compartments and each compartment is modelled as a CSTR, as shown in **Erreur ! Source du renvoi introuvable.** (a). A gaseous stream, made up of ethylene, hydrogen, nitrogen, and ICA is fed to CSTR 1. Condensed ICA can be injected at any point in the reactor, although it is a common practice that this is injected at the bottom of the bed alongside the gas. While the polymer is shown being recovered from CSTR 1 in this Figure,

it can be assigned to any of the compartments in the model. Similarly, the catalyst or prepolymer stream can be fed to any CSTR compartment as well. In each compartment, the gas fluidizes the bed of particles, and drags a portion of the polymer to the compartment above, while the remaining particles fall to the compartment below. Once the gas and solids reach the disengagement zone, the superficial gas velocity drops due to a larger reactor diameter. As a result, the majority of the solids that enter the disengagement zone fall back into the fluidized bed (CSTR *n*), but a small fraction can eventually leave the reactor, entrained by the gas. **Erreur ! Source du renvoi introuvable.** (b) is a simplification of **Erreur ! Source du renvoi introuvable.** (a), where the particles are not allowed to fall from one compartment to the compartment immediately below, rather they are always dragged to the compartment above. Once the solids reach CSTR *n*, a fraction moves up to the disengagement zone, dragged by the passing gas, while the remaining solids fall directly to the bottom of the reactor (CSTR 1) [23]. This simplification allows one to significantly reduce computation times and reduce the number of streams between compartments, but at the cost of a less realistic picture of FBR operation. In this work, a comparative exercise is performed which allows to see the difference between the two approaches.

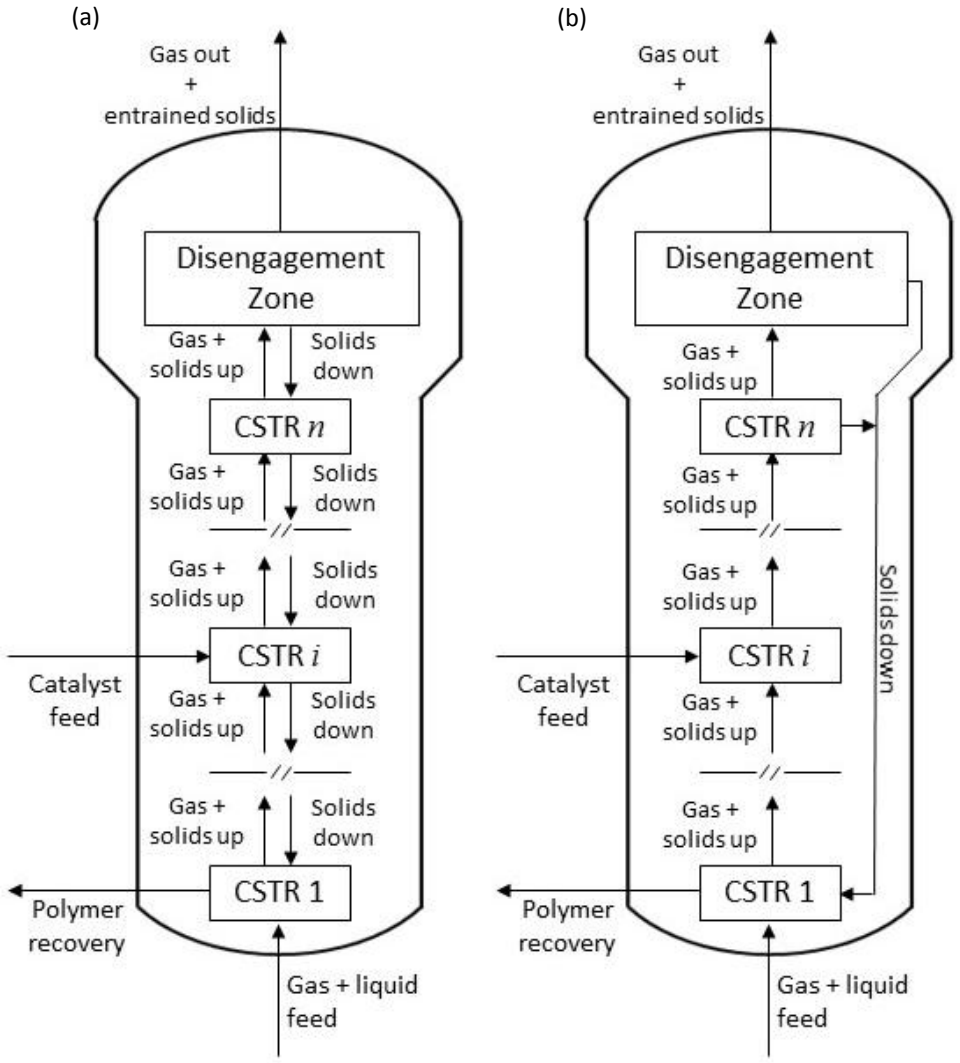

Figure 2. Diagram of the modelling structures for: (a) complete model and (b) simplified model.

2.2 Kinetic Modeling

The kinetics of gas-phase polyethylene polymerization over heterogeneous Ziegler-Natta catalyst has been extensively studied [2], [14], [24]–[27]. As the goal of the present study is to better understand how ICA is distributed in the reactor and its influence on things like the temperature profile of the bed, production rate and trends in terms of how the ICA can influence the molecular weight, a simplified kinetic scheme has been employed to describe the polymerization kinetics over a multiple-site Ziegler-Natta catalyst. We have therefore not included site activation

and deactivation reactions, transfer to alkyl, etc. in the kinetic scheme. The main steps included here are shown in Table 1.

Table 1. Mechanism for hydrogen effect on the polymerization rate of ethylene [24]. The subscript *k* represents the active site type.

Step	Chemical Equations	Rate Constant	Description
Propagation	$P_{\mathrm{n}}^{k} + M \rightarrow P_{\mathrm{n+1}}^{k}$	k_p^k	Main polymerization reaction step. The active chain of length n, P_{n}^{k}, reacts with an additional monomer molecule, M, increasing its chain length by one.
Transfer to H_2	$P_{\mathrm{n}}^{k} + H_2 \rightarrow P_H^k + D_n^k$	k_{tH}^k	Growth termination reaction of live polymer chains, forming dead polymer chains, D_n^k, and generate low-reactivity metal hydride sites, P_H^k.
Initiation of P_H^k	$P_H^k + M \rightarrow P_1^k$	k_{iH}^k	Initiation of P_H^k sites with monomer, which starts a new live chain, P_1^k

Equation (1) describes the polymerization rate, R_p,$\left(R_p \equiv mol \cdot {m_{cat}}^{-3} \cdot s^{-1}\right)$ according to the steps in Table 1.

$$R_p = \sum_{k=1}^{N_s} [S^k] \frac{k_p^k [M]}{1 + \frac{k_{tH}^k [H_2]}{k_{iH}^k [M]}} \quad (1)$$

Where $[S^k]$ is the concentration of active sites of type *k* and N_s is the number of different active sites considered. The kinetic parameters considered in this study are shown in Table 2. It is

important to mention that the effect of temperature on propagation rate constant was accounted for by using Arrhenius Law.

Table 2. Kinetic Parameters used in this study [24], [28].

	Units	Active site 1	Active Site 2
$k_{p,0}^{k}$	m^3/(mol.s)	180	220
E_a^k	J/mol	42000	42000
k_{tH}^{k}	m^3/(mol.s)	0.07	1.01
k_{iH}^{k}	m^3/(mol.s)	2	4
Initial Catalyst Active Site Concentration (C_0*)	mol/m^3_c	0.52	0.52
Active site fraction	(-)	0.3	0.7

The instantaneous molecular weight distribution for a multiple site can be easily obtained from the following equations [24]:

$$w_j(r) = \sum_{k=1}^{N_s} m_{k,j}\left(2.3026\, r^2 {\tau_{k,i}}^2 e^{-r\tau_{k,i}}\right) \quad (2)$$

Where j is the compartment number, r number chain length and $m_{k,j}$ and $\tau_{k,j}$ are obtain with equation **Erreur ! Source du renvoi introuvable.**a) and **Erreur ! Source du renvoi introuvable.**b).

$$m_{k,j} = \frac{R_{p,k}}{\sum_{j=1}^{N_s} R_{p,j}} \quad (2a)$$

$$\tau_{k,j} = \frac{k_{tH}^{k}[H_2]}{k_p^k[M]} \quad (2b)$$

The above equations provide a description of the instantaneous molecular weight distribution in a given compartment. To account for the different conditions in each compartment, the molecular weight distribution of the recovered polymer is obtained as per expression (3)**Erreur ! Source du renvoi introuvable.**, if the elutriation is negligible:

$$w(r) = \sum_{j=1}^{N} w_j(r)\left({Q_{pol,j}}/{\sum Q_{pol,j}} \right) \quad (3)$$

Where $Q_{pol,j}$ is the polymer production rate in each compartment.

2.3 Thermodynamic Model

The presence of ICA changes the solubility of ethylene in the amorphous phase of the polymer through a phenomena known as the *co-solubility effect* [29]–[31]. This means that even if the solubility of binary systems can be modelled with simple models like Henry's law under certain conditions, the thermodynamics of polymer systems is in fact non ideal. In cases such as those of interest in this work, it is necessary to use a thermodynamic model that accounts for interactions between the different components as soon as more than one penetrant is considered. As mentioned above, Alves *et al* [18] have shown that adding reasonable quantities of an ICA can reduce the average residence time of the reactor by more than half because of the co-solubility effect. Furthermore, the authors have shown that not accounting for the solubility effects results in predicting the wrong trends in terms of production rate and catalyst mileage when comparing different ICAs. Therefore, accurately modelling the solubility of ethylene and how its effected by the presence of the ICA is of the upmost importance. In this work, the ternary system Ethylene(1)/ICA(2)/PE(3) was modelled with the Sanchez-Lacombe Equation-of-State (SL-EoS).

The polymer chains are treated as a set of connected beads on a lattice, where the presence of empty sites is permitted in the lattice, but the lattice size is fixed [32]. Consequently, changes in volume are controlled by changes in the number of holes [33].

For a polymer liquid, the SL-EoS in terms of reduced variable is given by:

$$\bar{\rho}^2 + \bar{P} + \bar{T} \cdot \left[\ln(1-\bar{\rho}) + \left(1 - \frac{1}{r}\right) \cdot \bar{\rho}\right] = 0 \quad (4)$$

Where $\bar{\rho}$, $\bar{P}$, $\bar{T}$ are the reduced density, pressure and temperature, and are defined as:

$$\bar{T} = T/T^* \,,\ \bar{P} = P/P^*,\ \bar{\rho} = \rho/\rho^* \quad (5)$$

Here, T^*, P^* and ρ^* are, respectively, the characteristic temperature, pressure and close-packed mass density, which completely characterize a pure fluid. r is the number of sites a molecule occupies in the lattice. Any thermodynamic property can be utilized to determine these parameters, but several authors have published tables where these molecular parameters are made available [32]. This (and other equations of state) rely on a set of interaction parameters, k_{ij}, that need to be established for each system (polymer + penetrants) of interest. The k_{ij} is dependent on the solute(s)-polymer system used and correlated to the temperature and can be fitted when experimental data is available [33]. Solubility data is often used for this end as it is commonly found for binary systems, and while it is still scarce for more realistic mixtures, some data can be found for ternary systems [34]. Details regarding the SL-EoS parameters and solution strategy can be found elsewhere [28], [35]. The values of k_{ij} used in this work were taken from the correlations made available by Alves *et al* [10] and the values presented by Ben Mrad [34].

2.4 Single Particle Modeling

Gas phase polymerization of ethylene is performed using supported catalysts (or prepolymerized supported catalysts). As soon as the particles are injected into the reactor, polymerization begins

on the surfaces of the pores of the support, immediately covering the active sites with a layer of polymer. As the polymer layer accumulates, the initial support material fragments, and, ideally, the catalyst particle is transformed into a single polymer. Monomer(s), hydrogen, and other materials continue to sorb in the polymer layer, diffuse to the active sites where the polymerization continues until the particles are withdrawn from the reactor. As more polymer accumulates, the particle grows by expansion. Mass and heat transfer effects can be important in determined concentration and temperature profiles in the growing particle, and as these can be influenced by the amount and type of ICA present in the system, it is important to include particle level models.

To estimate the concentration profile in the particles, the well-known diffusion reaction equation was used:

$$\frac{\partial C_{i,p}}{\partial t} = D_{i,eff}\ \frac{1}{r^2}\frac{\partial}{\partial r}\left(r^2\frac{\partial C_{i,p}}{\partial r}\right) - R_p \tag{6}$$

boundary conditions are:

$$\frac{\partial C_{i,p}}{\partial r}(r = 0, t) = 0 \tag{6a}$$

$$D_{i,eff}\frac{\partial C_{i,p}}{\partial r}\big(r = R_L(t)\big) = S_{i,pol} \tag{6b}$$

Initial Condition:

$$C_{i,p}(r, t = 0) = S_{i,pol} \tag{6c}$$

Where $C_{i,p}$ is the evolving concentration of species inside the pore space of the pseudo-homogeneous phase that makes up the particle, t is the polymerization time, r is the radial position in the particle, $D_{i,eff}$ is the effective diffusion of the species in the macroparticle (*i.e.* through the pseudo-phase composed of pores and polymer), and R_p is the polymerization rate.

$S_{i,pol}$ is the solubility of a given species in the polymer phase, given by the Sanchez-Lacombe EoS. Equation (6) was applied to both ethylene and hydrogen, to obtain their concentrations at the active sites.

The effective diffusion is the result of two complementary processes:

- Diffusion of the gases though the particle's pores;
- Diffusion of the penetrants the solutes through amorphous phase of the semicrystalline polymer (the crystalline phase is considered to be impenetrable [36]).

The effective diffusion was calculated as described by Kanellopoulos *et al* [37]:

$$D_{i,eff} = \frac{\varepsilon}{\tau^2} D_{i,g} + (1-\varepsilon)(1+3\varepsilon) D_{i,pol} \quad (7)$$

where τ is the tortuosity factor and ε is the particles porosity, $D_{i,g}$ diffusivity of species i in a multicomponent gaseous system, calculated according to Chapman-Enskog theory [38] and shown in supporting information. $D_{i,pol}$ is the diffusivity of penetrant i in the semicrystaline polymer, calculated according to Alves *et al.*[10]. It is important to note that the ICA has been shown to increase the diffusivity of ethylene in the amorphous phase of the polymer, so this effect needs to be accounted for better model predictions [10]. However, the diffusion of hydrogen is assumed to be unaffected by the presence of ICA and has been calculated for the system hydrogen/polymer. The value of τ is assumed to be 10, which has been used in the past for compact PE particles. [39][40].

Similarly, the temperature profile of the particles was obtained:

$$\rho_p C_p \frac{\partial T_p}{\partial t} = k_c \frac{1}{r^2} \frac{\partial}{\partial r}\left(r^2 \frac{\partial T_p}{\partial r}\right) - (\Delta H_p) R_p \quad (8)$$

Boundary Conditions:

$$\frac{\partial T_p}{\partial r}(r = 0, t) = 0$$

$$k_c \frac{\partial T_p}{\partial r}(r = R_L(t), t) = h(T_b - T_p) \tag{8a}$$

Initial Condition:

$$T_p(r, t = 0) = T_{p,0} \tag{8b}$$

$$\tag{8c}$$

where ρ_p is the particle density, C_p the heat capacity of the particle, T_p the local particle temperature, k_c the particle effective thermal conductivity and ΔH_p the heat of polymerization. T_b the bulk temperature and $T_{p,0}$ is the initial particle temperature. The convective heat transfer coefficient, h, was calculated with the Nelson-Galloway correlation as suggested by Floyd *et al.* [41], shown in supporting information. k_c is assumed to be 0.48 W/(m K) [36].

2.5 Population Balance Equations

Continuing with the assumption that the compartments are perfectly back-mixed CSTRs, if no agglomeration or attrition is considered, the steady state population balance equation for the particles that ranges in size from D to $D + \Delta D$ is given as [42]:

$$\begin{pmatrix} particles\ entering \\ compartment\ with\ size \\ between\ D, D + \Delta D \end{pmatrix} + \begin{pmatrix} particles\ growing \\ by\ polymerization \\ to\ size\ D, D + \Delta D \end{pmatrix} - \begin{pmatrix} particles\ exiting \\ compartment\ with\ size \\ between\ D, D + \Delta D \end{pmatrix}$$
$$- \begin{pmatrix} particles\ outgrowing \\ by\ polymerization \\ a\ size\ D, D + \Delta D \end{pmatrix} - \begin{pmatrix} particles\ exiting\ compartment \\ due\ to\ elutriation \\ with\ size\ between\ D, D + \Delta D \end{pmatrix} = 0 \tag{9}$$

It is important to note that, due to the well-mixed assumption, the particle size distribution of the particles in the polymer recovery stream will be identical to that of the compartment where the

stream is recovered. Furthermore, equation (9) shows that elutriation is only possible from the n^{th} CSTR compartment (top of the bed). For all other compartments, there is no elutriation. Expressing the terms of equation (9) as a function of number density and the corresponding mass flowrate in the different streams, equation (10) can be obtained [43]:

$$F_{in,j}P_{in,j}(D) + \frac{3w_{bed,j}}{D}\psi(D)P_{out,j}(D) - F_{out,j}P_{out,j}(D) - w_{bed,j}\frac{d\left[\psi(D)P_{out,j}(D)\right]}{dD} - F_{e,j}P_{e,j}(D) = 0 \quad (10)$$

Where F represents a mass flowrate, P represents a number function density, D is the particle diameter, w_{bed} is the compartment bed weight (which depends on compartment height) and $\psi(D)$ is the rate of particle growth. The subscripts *in* and *out* represent respectively, streams that enter and exit the compartment. The subscript *e* refers to the elutriation stream and *j* refers to the compartment number.

Equation (10) can be numerically solved when its terms are determined as follows:

- Rate of particle growth [42][21]:

  $$\psi(D) = \frac{{D_i}^3}{3(1-\varepsilon)D^2}\frac{\rho_i}{\rho}R_p \quad (11)$$

  Where D_i is the initial particle diameter, ε is the particle porosity, ρ is the particle density and R_p is the reaction rate.

- Flux of particles carried out of the bed due to entrainment [22], [43]:

  $$F_{e,j}P_{e,j}(D) = w_{bed}K_e(D)P_{out,j} \quad (12)$$

  Where K_e is the elutriation rate constate, given as [43], [44]:

$$K_e = 23.7\rho_g u_0 \exp\left(-\frac{5.4u_t}{u_0}\right)\frac{A_{bed}}{w_{bed}} \quad (13)$$

- To account for particle size distribution in the feed stream [42]:

$$P_{out,j} = \int_{D_{min}}^{D} P_{out,j}(D, D_i)P_{in,j}(D_i)\, dD_i \quad (14)$$

Where D_{min} is the smallest particle that grow to size D, $P_{out,j}(D, D_i)$ is the fraction of particles of size D grown from particles of size D_i and $P_{in,j}(D_i)$ is the fraction of particles of size D_i on the inlet feed.

The steady state population balance could be obtained (equation (15)) by substituting equations (11) to (13) in equation (10). This equation, applied to each compartment, has been numerically solved following the approach of Selçuk *et al.*[45].

$$\frac{dP_{out,j}(D)}{dD} = \frac{1}{w_{bed,j}\psi(D)}\left(F_{in,j}P_{in,j}(D) - F_{out,j}P_{out,j}(D) - F_{e,j}P_{e,j}(D)\right) + \frac{P_{out,j}(D)}{D} \quad (15)$$

2.6 Compartment height

Since the objective of this work is to model the effects of ICA on reactor operation, it is of interest to be able to model the distribution of liquid in the reactor when running in fully condensed mode, the axial temperature profile in the bed, as well as the co-solubility effects on the solubility of ethylene in the amorphous polymer. As discussed above, the gas solubility in the polymer and the Sanchez-Lacombe interaction parameter (k_{ij}) are dependent on the temperature. We propose to define the compartment height in such a way as to ensure that the temperature changes between inlet and outlet of each compartment does not provoke a difference of more than 10% in the solubility of ethylene in the amorphous polymer.

The changes in ethylene solubility as a function of temperature in the ternary system ethylene/n-pentane/polyethylene calculated are shown in Figure 3. The partial pressure of ethylene is kept constant at 7 bar. The pressure of n-pentane is equal to the vapor pressure at each temperature, because as shown by Zhou *et al.* [16], the biggest gradient of temperature occurs at the bottom of the bed, where the gas-liquid-solid phases co-exist.

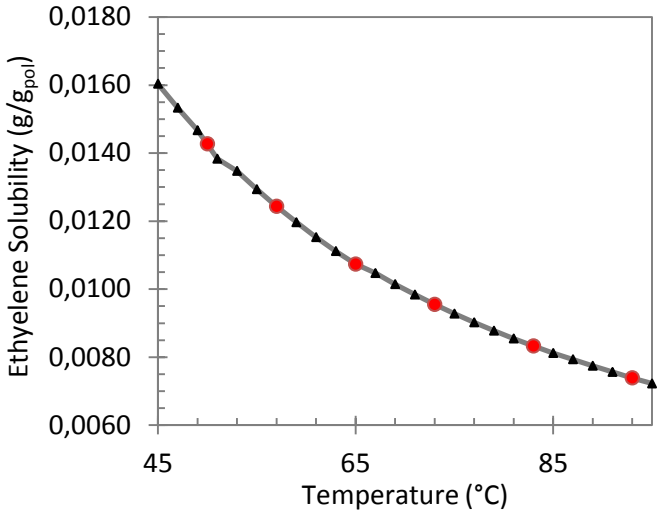

Figure 3. Relationship between the solubility of ethylene in the amorphous phase of the polymer and temperature. The line represents the calculated values for ethylene solubility, obtained with the SL-EoS, while the dots represent variation in 10% in solubility.

Analyzing the data in Figure 3, it is possible to see that at lower temperatures, changing the temperate by 5°C provokes a change of 10% in the solubility of ethylene. Taking into account the industrial bed temperature profiles presented by Zhou *et al* [16] and in patent [46], the bed height was discretized in such a way that the maximum temperature difference between intervals is 5°C. Figure 4 shows the temperature profiles in the bed in respect to bed height for the case of dry mode (i.e. no ICA present) operation, where the heat transfer is the least favorable and therefore has the steepest temperature increase at the bottom of the reactor. The continuous line shows the

industrial data while the dots represent the 5 °C increments in the bed temperature, and denote where a new compartment should start.

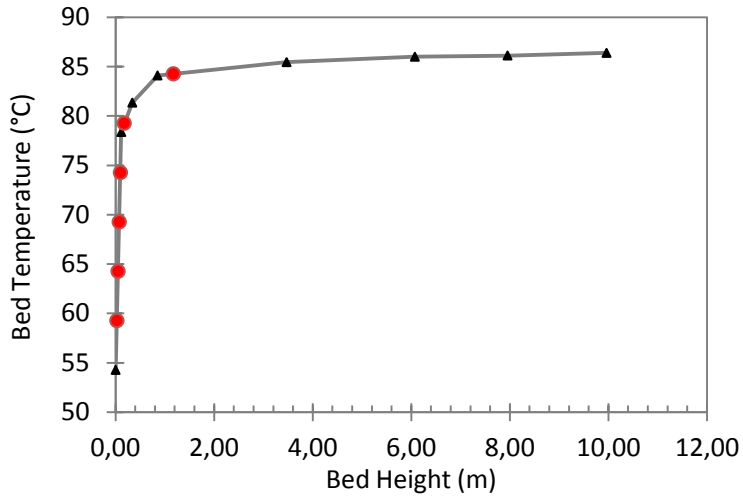

Figure 4. Temperature profiles in the bed for dry mode (data published by Zhou *et al* [16]). The red dots represent 5°C increments in the temperature and represent the height of the compartments.

Figure 4 shows that the bottom of the reactor, where the gas-liquid-solid phases co-exist, needs to be modelled with at least 6 compartments. To ensure that the top compartment has no liquid, *i.e.* only gas and solid phases are present, an additional compartment has been added. The height of the compartments used in this work is given in Table 3. The total bed height was chosen equal to 13.5 m based on information from a publication by Zhou *et al*. [16] so that we could compare our simulated temperature profiles with the industrial data they provided. Simulations (see below) were run with 16 compartments to validate this approach.

Table 3. Compartments height for a total height bed of 13.5m.

CSTR #	Compartment	bed height (m)

	height (m)	
1	0.03	0.03
2	0.02	0.05
3	0.02	0.07
4	0.02	0.1
5	0.08	0.2
6	1.0	1.2
7	1.3	2.5
8	11.0	13.5

Unless stated otherwise, the inlet of catalyst has been set at 2 m, meaning that it is introduced in the 7th compartment, the polymer recover occurs at 1 m in the 6th compartment and the liquid is injected alongside the gas in compartment 1.

2.7 Evaporation Model

The liquid is distributed to the reactor in the form of small droplets, either using specialized spray nozzles, deflector plates or other technology [47][48]. In this work, a uniform droplet size distribution was assumed. The majority of the simulations, a droplet diameter (d_p) of 200 µm [49]–[52] was used, although a discussion on the effects of droplet size is also be presented. The droplet evaporation rate is was described by Bird *et al* [38]:

$$E_\infty = K_{xm}\left(\pi {d_p}^2\right)\frac{x_{ICA,0} - x_{ICA,\infty}}{1 - x_{ICA,0}} \quad (16)$$

In the above equation, E_∞ represents the evaporation rate (kg/s), $x_{ICA,0}$ is the mole fraction of the ICA vapor at the droplet surface and $x_{ICA,\infty}$ is the mole fraction of ICA in the bulk of the gas-phase. K_{xm} is the mass transfer coefficient, calculated for the case of forced convection around spheres [38]. The details concerning the estimation of K_{xm} are shown in supporting information.

Assuming that the total number of droplets remains constant, the total evaporation for each compartment ($F_{ICA,evap}$) and can be obtained by equation (17), where H_j is the compartment height and $m_{droplet,j}$ is the mass of one droplet in compartment j.

$$F_{ICA,evap} = \int_0^{H_j} E_{\infty,j} \frac{W_{bed,j}}{hm_{droplet,j}} dh \tag{17}$$

3 Results

The data used across all simulations is shown in Table 4.

Table 4. Data used for all simulations

Parameter	Units	Value	Ref
Reactor Diameter (d)	m	4.75	[19]
Reactor Bed Height (H_b)	m	13.3	[19]
Catalyst Density (ρ_c)	kg/m^3	2300	[28]
Catalyst Heat Capacity ($Cp_{,c}$)	J/(kg.K)	2000	[28]
Polymer Heat Capacity ($Cp_{,p}$)	J/(kg.K)	2000	[28]
Heat of Reaction (ΔH)	J/mol	-107600	[28]
Fluidized Bed Porosity ($\varepsilon_{f,}$)	-	0.6	[18]

3.1 Model Validation

Model validation was carried out in two phases: comparison with patent data [19], found for the homopolymerization of ethylene in the presence of gaseous ICA and through the replication of the industrial temperature profiles presented by Zhou *et al* [16] for condensed mode operation.

Both validation methods were performed using the complete model, shown in **Erreur ! Source du renvoi introuvable.** (a).

3.1.1 Patent data validation

In the examples provided for the homopolymerization of ethylene on patent US 6864332 B2 [19] certain runs contain a mixture of ICAs and ethylene. This implies that for thermodynamic modelling, a quaternary system should be considered. However, there is a lack of experimental solubility data that would allow fitting of the data the Sanchez-Lacombe interaction parameter (k_{ij}). Therefore, the method for accounting for two ICAs described in our previous work has been employed [18]. Furthermore, the effects of co-diffusion could not be modelled since we did not have the necessary thermodynamic information, so the single particle model was not applicable at this stage. Table 5 shows the comparison between the results presented in examples 7A and 7C of reference [19] and the results obtained in the simulations.

Table 5. Model validation with example 7A and 7C of patent [19]. The outlet temperature is the temperature of the gas withdrawal at the top of the reactor.

		7A	**Sim. 7A**	**Δ (%)**	**7C**	**Sim. 7C**	**Δ (%)**
PE Production Rate	(tonne/h)	16	15.7	-2%	28.9	28.8	0%
Inlet Temperature	(°C)	35	35	-	35	35	-
Outlet Temperature	(ºC)	88	87	-1%	88	87	-1%
Superficial Velocity	(m/s)	0.75	0.75	0%	0.75	0.75	0%

Productivity	(g_{pol}/g_{cat})	53,650	54,905	2%	29,700	29,691	0%
Residence Time	(h)	4.6	4.8	8%	2.5	3.1	19%

These preliminary simulations suggest that the model manages to capture the observed temperature gradients and fluctuations in productivity reasonably well.

3.1.2 Temperature Profile Validation

The temperature profile in the bed was compared to the industrial results published by Zhou et al. [16]. Since no kinetic constants or catalyst feed rate were provided by these authors, the catalyst feed rate was adjusted to obtain similar production rates. The inlet conditions are shown in Table 6, as well as the obtained production rate and the liquid height. The liquid height is the height of the bed where the co-existence of gas, liquid and solid phases is observed. Above this height is assumed that only gas and solid phases are present. These values taken from Zhou *et al.* [16] and are a result of their modelling work, not experimental values. Furthermore, in their work, they considered that the liquid coated the particles and therefore the size of the droplet was that of the size of the particle [16].

Table 6. Model validation with experimental data provided by Zhou *et al*. [16]. Liquid height refers to the bed height where three phases (gas/liquid/solid)co-exist. The values calculated with the proposed model are noted as “Sim”.

		Liquid Content (%)				
		0	2.3	8.1	15.9	20.5
Inlet Temperature	(ºC)	53.8	54.8	54.1	46.8	44.5
Recycle gas flowrate	(tonne/h)	1100	1118	1128	1200	1229
Production rate	(tonne/h)	17.72	19.2	25.1	37.6	46.0
Sim production rate	(tonne/h)	16.9	20.0	25.9	35.0	45.0
Δ (%)	(-)	5%	4%	3%	7%	6%
Liquid height	(m)	0	0.43	1.02	2.1	2.4
Sim liquid height	(m)	0	0.6	1.2	1.8	2.1
Δ (%)	(-)	0%	46%	17%	17%	13%

The predicted values for the production rate present only small differences to the industrial data provided in the paper. While the liquid heights simulated with the model presented here are slightly different from the simulated results proposed by Zhou et al., the trends are quite encouraging. Furthermore, the droplets of liquid in our simulations are smaller than those in the cited reference, as those authors they considered that the liquid coated the particles and therefore the size of the droplet was that of the size of the particle. Furthermore, the model of Zhou *et al*. [16] assumes that the bottom of the bed where the liquid is present moves in plug flow, whereas the current model allows for back-mixing of the bottom compartments, so the physical description of the reactor is different at this level.

Figure 5 shows the bed temperature profile for dry mode and for a liquid content of 15.8%. The temperature profiles for the other liquid contents can be found in supporting information.

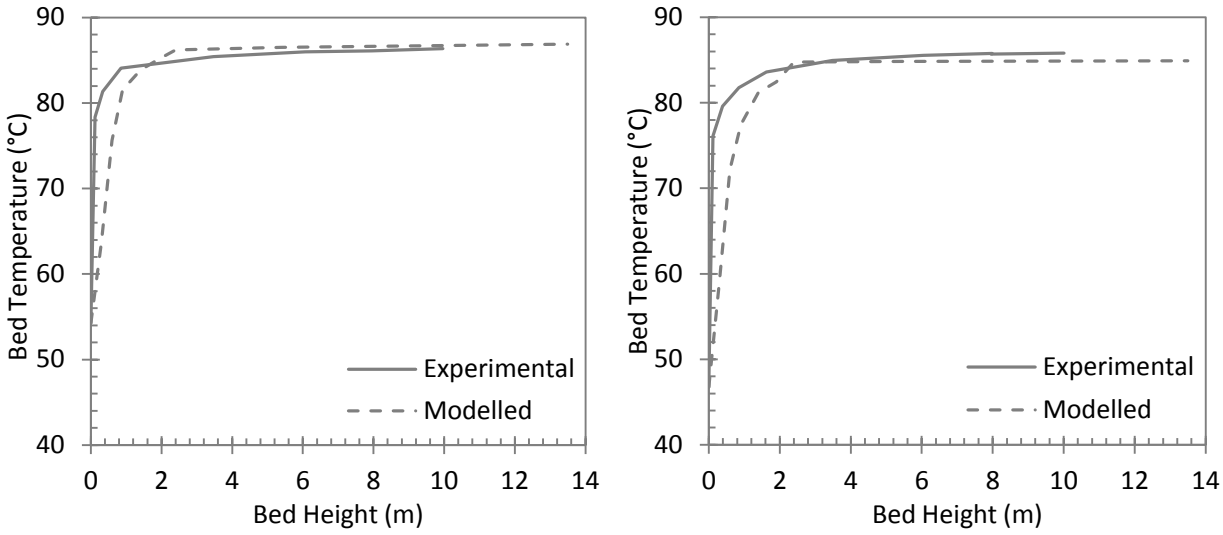

Figure 5. Bed Temperature Profile for: (a) dry mode (i.e. no liquid fraction); (b) liquid fraction of 15.9%. industrial data obtained from Zhou et al. [16].

From these comparisons, we can be satisfied that the model developed here is able to describe the experimental temperature profiles reasonably well for both the dry and condensed mode, especially considering that we have no information on the kinetics of the catalyst used in reference paper. The model can predict the trend for the temperature profiles, slightly deviating from the experimental values at the bottom of the bed. We can therefore assume that this model is valid and fit to describe the reactor behavior of a FBR for polyethylene production working under condensed mode.

3.2 Case Studies

For the following case studies the inlet conditions are shown in Table 7.

Table 7. Inlet parameters for the simulations.

Parameter	Unit	Value
Inlet gas temperature	°C	54
Bulk temperature	°C	85
Inlet gas flow rate	mol/s	10000
Superficial Velocity	m/s	0.75
Reactor Abs. pressure	bar	22.4
Ethylene partial pressure	bar	7
Hydrogen partial pressure	bar	1
Nitrogen partial pressure	bar	14.4 to 12.6

3.2.1 Case study I – Complete Vs Simplified Model

The simulations presented bellow aim to show the differences that one might obtain when employing a simplified approach. The complete model and the simplified approach, shown in Figure 2, have been compared. The results in terms of particle size distribution for both approaches are shown in Figures 6 and 7, for two different superficial velocities and no ICA present. The temperature at the top of the reactor has been kept constant at 85°C in both cases by adjusting the catalyst feed rate. Figure 6 shows the particle size distribution at the top and bottom compartments of the fluidized bed for a gas superficial velocity of 0.75 m/s. At this superficial velocity, both models predict similar particle size distributions. Furthermore, no bed segregation is observed, as the particle size distribution at the top is similar to that of the bottom of the bed, which is expected and in well agreement with other authors [21], [23].

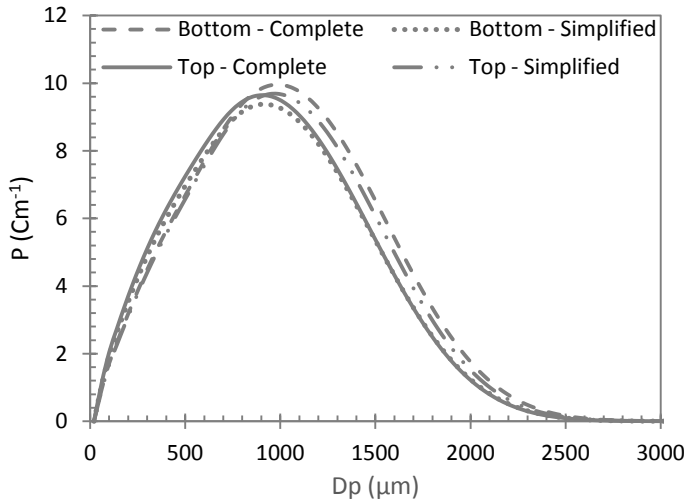

Figure 6. Particle size distribution for the top and bottom compartments at a gas superficial velocity of 0.75m/s.

Figure 7 reveals that decreasing the superficial gas velocity leads to not only bed segregation, but to slightly different predictions from the two modelling approaches. It becomes clear that at lower superficial velocity the particle size in the bed is no longer homogenous, with the bigger particles not being fluidized and remaining at the bottom of the bed. The simplified approach predicts smaller particles at the bottom than the complete approach, as a result of instantaneous recycling of the particles to the bottom of the reactor. Furthermore, at the top of the bed, the simplified approach predicts bigger particles than the complete model. This means that the bed segregation, as calculated by the simplified approach is milder than that predicted by the complete approach.

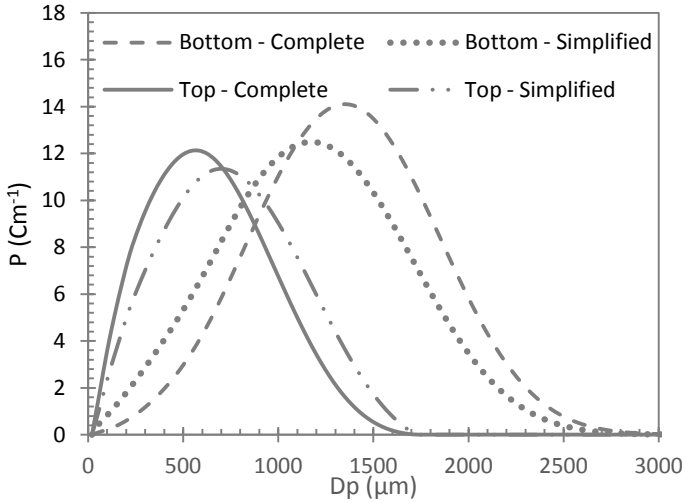

Figure 7. Particle size distribution for the top and bottom compartments at a gas superficial velocity of 0.25m/s.

The calculated production rates for both superficial velocities is shown in Table 8. Both modelling approaches predict similar values for each superficial velocity. However, there is a 6% deviation between the complete and simplified model when the superficial velocity is 0.25 m/s. The same is true for the temperature profiles: both approaches are very similar, as shown in Figure 8, but the temperature profiles predicted by both approaches diverge slightly for the lower superficial velocity. In fact, the simplified model seams to predict a slightly higher temperature profile than the complete model.

Table 8. Comparison of the production rate calculated by both modelling approaches and at two different superficial velocities.

Superficial velocity (m/s)	**Complete model (ton/h)**	**Simplified model (ton/h)**	**Δ (%)**
0.75	11.19	11.21	0.2
0.25	4.04	4.32	6.5

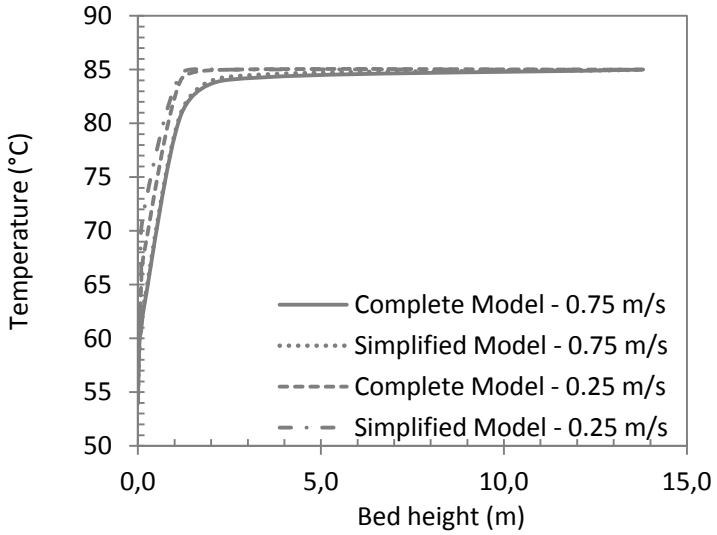

Figure 8. Temperature profiles for both superficial velocities and modelling approaches.

From the results above, it becomes clear that the only major difference between these model is the particle size distribution predictions. Therefore, if bed segregation is the subject of interest in a modelling exercise, the complete approach might be better suited. However, at the industrially pertinent gas velocities, the two approaches appear to predict very similar results. We will use the complete model in the rest of this paper for the sake of completeness.

3.2.2 Case study II – Effects of Number of Compartments

The effects of the number if compartments on the particle size distribution and temperature profile of the reactor have been studied. The superficial velocity of the gas was kept at 0.75m/s and the complete approach has been employed. Furthermore, no ICA was used in these simulations. In one simulation, the number of compartments are those shown in Table 3 for a total of 8 compartments plus a disengagement zone, and in a second simulation 16 compartments plus a disengagement zone were used, where each compartment has half the height of those shown in Table 3. This is a crucial exercise, as the definition of compartment height is not

without its challenges. To the best of our knowledge, no other study in the open literature has discussed in detail the importance of compartment height or proposed criteria to define it.

The results in terms of particle size distribution are shown in Figure 9, while the results in terms of temperature are shown in Figure 10.

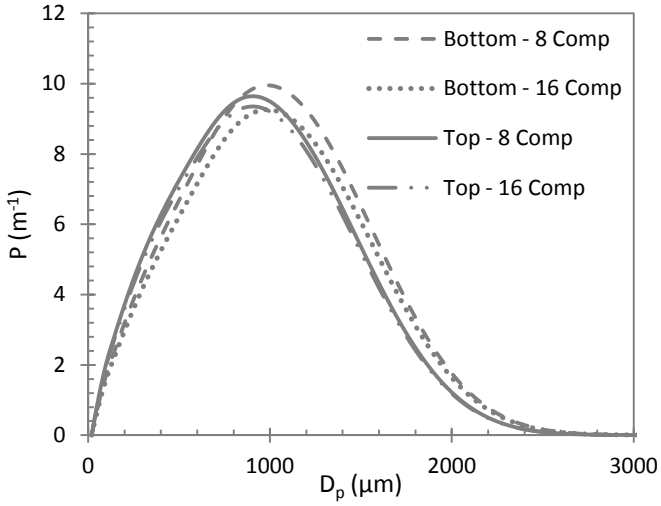

Figure 9. Effect of number of compartments on the particle size distribution for the top and bottom compartments.

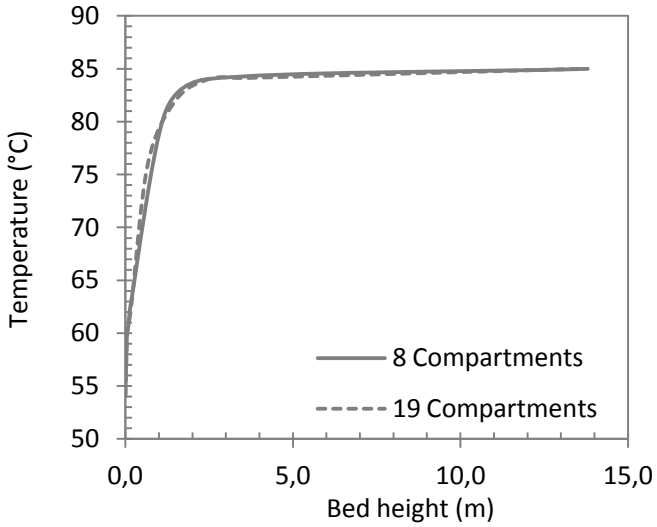

Figure 10. Effect of number of compartments on the temperature profile of the reactor.

The figures show that for the two sets of compartments simulates, the model predicts very similar results. Slight differences in the temperature profile and PSD are most likely caused but the catalysts being fed into a smaller compartment when the number of compartments is larger, and therefore staying shorter amounts of time in it. Nevertheless, there appears to be no significant difference as a function of the number of compartments, so the remainder of the simulations in this paper will be carried out with 8 compartments, since this requires significantly less computational time.

3.2.3 Case study III – Effects of n-pentane Vs n-hexane

The simulations presented in this section show how two different ICAs (n-pentane and n-hexane) impact the reactor behavior, production rate, and final product particle size distribution. The bulk temperature, meaning the temperature of the gas stream at the top of the reactor is kept at 85 °C, by changing the inlet catalyst feed rate. Table 9 shows the simulation results in terms of production rate, catalyst mileage, residence time, liquid height, and elutriated flowrate for different liquid contents and both ICAs.

Table 9. the simulation results in terms of production rate, catalyst mileage, residence time, liquid height, and elutriated flowrate for n-pentane and n-hexane with different liquid contents.

	W_{liq} (%)	n-Pentane	n-Hexane
Production rate (ton/h)	0	11	11
	5	20	18
	10	26	24
	15	31	32
Catalyst mileage (g/g)	0	2491	2491
	5	2388	3255
	10	1939	3002
	15	1574	2763
Residence time (h)	0	3.0	3.0
	5	2.0	2.7
	10	1.7	2.1
	15	1.5	1.8
Liquid height (m)	0	0.0	0.0
	5	0.7	0.9
	10	1.0	1.4
	15	1.3	1.9
Elutriated flowrate (ton/h)	0	0.11	0.11
	5	0.18	0.21
	10	0.32	0.35
	15	0.47	0.49

The results show that at equal mass fractions in the feed, n-pentane seems leads to higher production rates than n-hexane. n-Hexane provides a greater cooling effect than n-pentane, which leads lower temperatures on the bottom compartments and, therefore a lower production rate (this will be discussed further below). However, the catalyst mileage in both cases is very different. For the case of n-pentane, it decreases 37% when increasing the liquid content to 15%. For n-hexane, the catalyst mileage actually increases in comparison to the dry mode when small amounts of liquid are present. Still, the more liquid is added, the lower the catalyst mileage. This

is because n-hexane not only has more pronounced co-solubility effect, but it also has an important co-diffusion effect. Figure 11 (a) shows the ethylene concentration in the amorphous polymer for no ICA and for both n-pentane and n-hexane at 15% liquid fraction. It is clear that n-hexane increases the solubility of ethylene in the amorphous phase (higher concentration of ethylene at the surface of the particle), but it also shows that the co-diffusion effects ensure that the concentration of ethylene at the active sites is higher. Figure 11 (b) shows the importance of this co-diffusion effect. For both simulations the co-solubility effect of n-hexane was included, therefore we observe the same solubility at the surface of the particle. However, the concentration of ethylene at the active sites becomes lower as we move to the center of the particle if no co-diffusion effects are taken into account. Furthermore, if the co-diffusion is not included, the evolution of the catalyst mileage with the increased liquid content follows the trend seen for n-pentane (Figure 12)

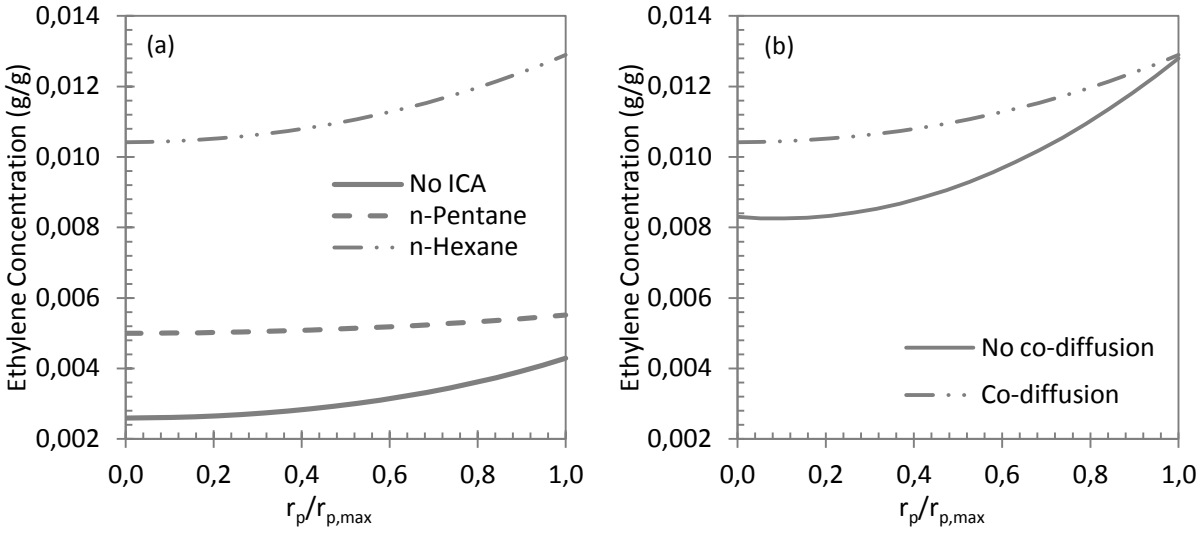

Figure 11. Concentration of ethylene in an average size particle for: (a) no ICA present and for n-pentane or n-hexane with a liquid fraction of 15%; (b) 15% liquid fraction of n-hexane with and without the co-solubility effects (both simulations account for co-solubility effects).

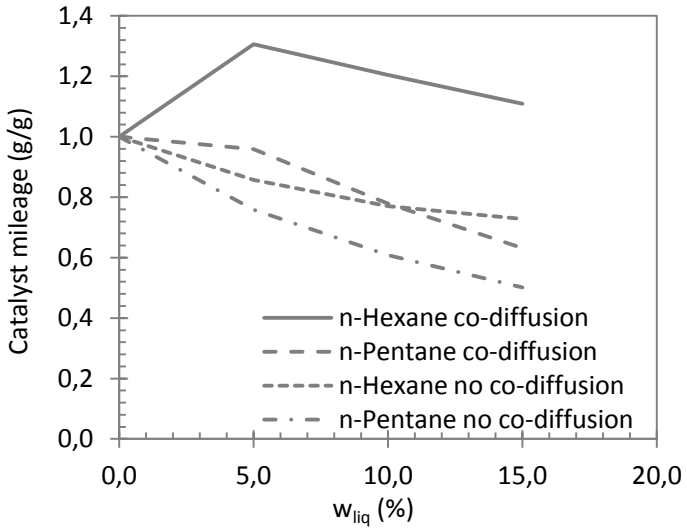

Figure 12. Effect of co-diffusion on normalized catalyst mileage for different n-hexane or n-pentane liquid contents.

In Table 9 it is also shown that the average residence time in the reactor decreases with increased liquid content, due to higher production rates. Furthermore, the increase in liquid content increases the rate of elutriation. This is because the liquid that is fed into the reactor rapidly evaporates and expands, increasing the superficial velocity of the gas at the top of the bed.

The results in terms of the effects of the two ICA in the temperature profiles of the reactor are shown in Figure 13, and inside the particles in Figure 14. Figure 13 (a) and (b) show that the higher liquid content, the less sharp the temperature gradient at the bottom of the reactor, with n-hexane having a more pronounced cooling effect (Figure 13 (c)). The effects of ICA in the temperature profile inside the particles of an average size is shown in Figure 14. The temperature gradients present the same shape in all cases, with temperature shifts due to different polymerization rates. This is an expected result, since the effects of heat of sorption/desorption of the ICA and potential ICA effects on the thermal properties of the particle have not been included, as the work of Alizadeh *et al* [53] has already showed that they can be dismissed.

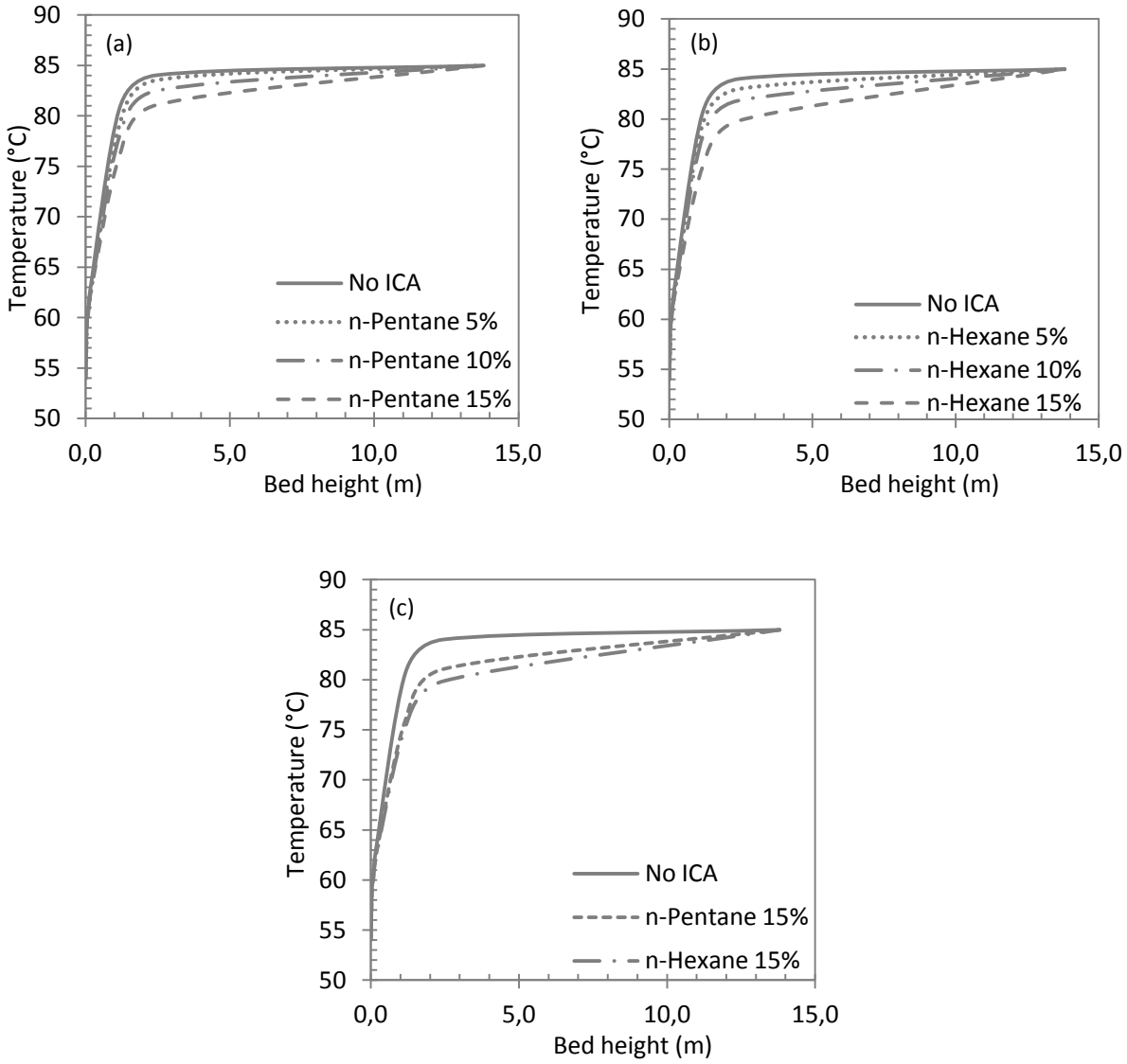

Figure 13. Temperature profiles in the bed for different liquid contents of n-pentane (a) or n-hexane (b) and a comparation between the effects of n-pentane and n-hexane with a liquid fraction of 15% (c).

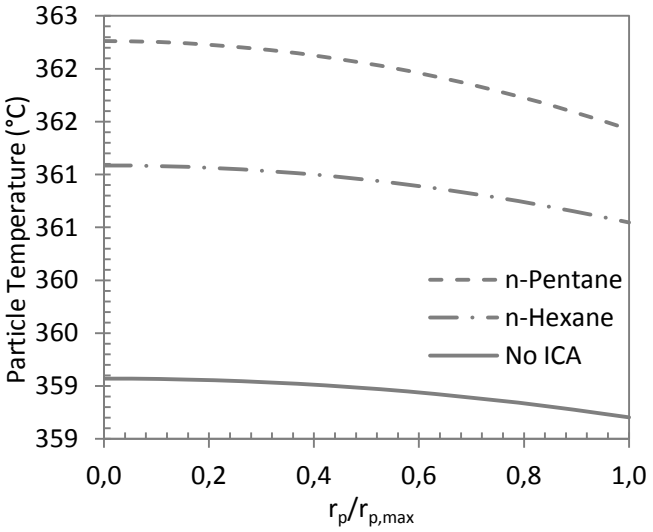

Figure 14. Particle Temperature ethylene in an average size particle when no ICA present, 15% liquid fraction of n-pentane or 15% liquid fraction of n-hexane.

The effect of both ICAs on the particle size distribution was also been investigated. Figure 15 shows the results of the final product PSD (*i.e.* the PSD of the compartment where the polymer has been recovered). The ICA is shown to slightly broaden the particle size distribution and to increase the average particle size.

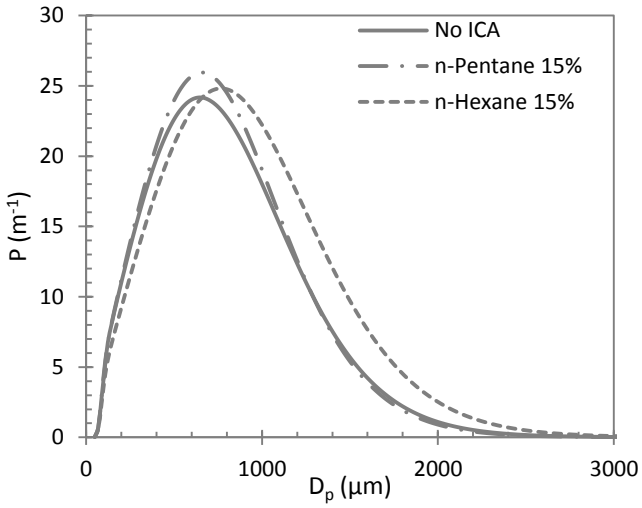

Figure 15. PSD of the final product for the case for no ICA, n-pentane or n-hexane with a liquid fraction of 15%.

3.2.4 Case Study IV – Effects of temperature in the presence of ICA

The effects of the temperature on the reactor production rate and catalyst mileage were investigated for a super-dry mode operation (i.e. no liquid) with n-hexane as ICA, with a partial pressure up to 0.6 bar.

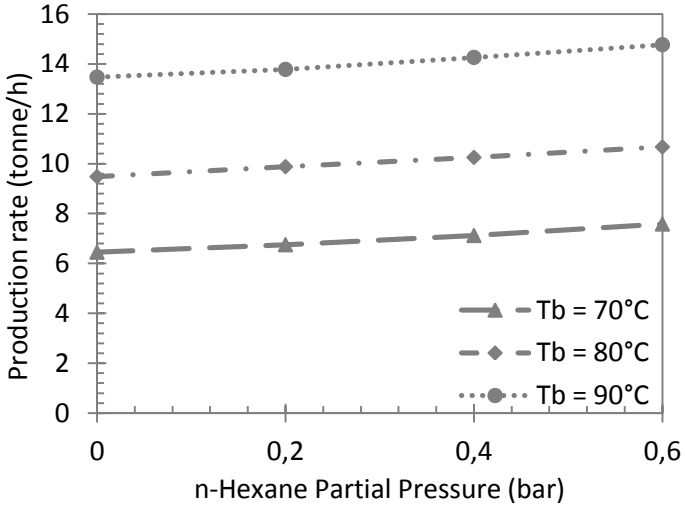

Figure 16. Effects of the temperature in the production rate of the reactor in the presence of n-hexane.

Figure 16 shows that the production rate of the reactor increases with the temperature and the increase of ICA. In Figure 17 however, it becomes clear that at lower temperatures there is an increase of catalyst mileage. This is an expected result, previously reported in a semi-batch experimental by Andrade [54]. At lower temperatures, the solubility of ethylene is higher and the co-solubility effect is stronger and therefore there are competing effects between these and the effects of temperature in the kinetic constants. This means that at 70°C the ICA has more influence over the reaction rate than at 90°C, as shown in Figure 18. Furthermore, Andrade [54] shows the effects on rate of reaction due to the presence of ICA are more noticeable at 70°C than at higher temperatures.

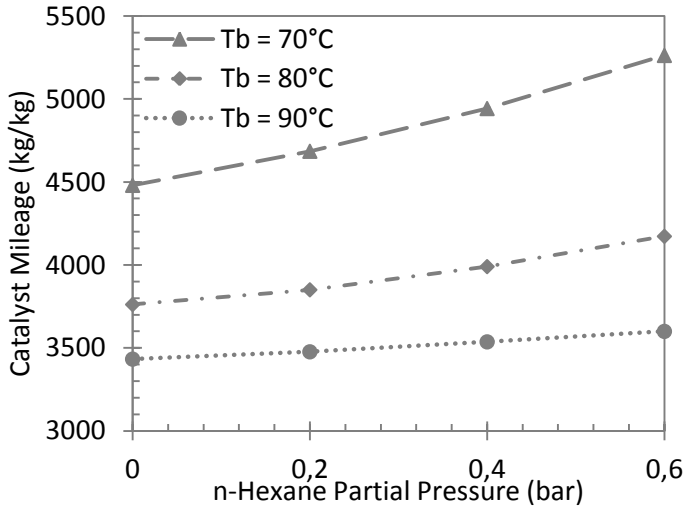

Figure 17. Effects of the temperature in the catalyst mileage in the presence of n-hexane.

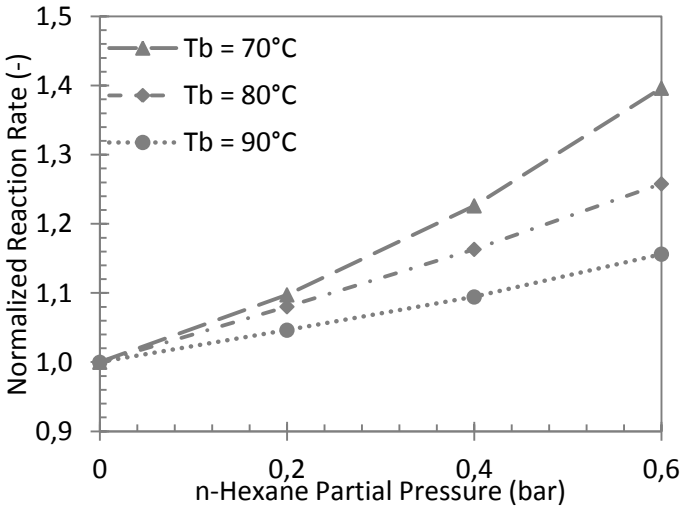

Figure 18. Effects on the temperature on the normalized reaction rate.

3.2.5 Case Study X – Effects of inlet temperature

The effects of inlet temperature on the condensed mode operation were investigated. For this, the dry-mode operation (i.e. no ICA) with an inlet temperature of 54°C is compared with a super dry mode operation, at the same inlet temperature, where the partial pressure of ICA is equal to the partial pressure of ICA. The temperature of the inlet feed is then decreased, while the amount of ICA remains the same, leading to the partially condensation of the ICA (see Table 10). n-Pentane was used as ICA in these simulations and all other reactor parameters are kept constant.

The results in terms of the production rate and catalyst mileage are shown in Table 10.

Table 10. ICA partial pressure, ICA liquid content, production rate catalyst mileage for different inlet temperatures.

Inlet T (°C)	**Inlet ICA partial pressure (bar)**	**W_{liq} (%)**	**Production rate (ton/h)**	**Catalyst mileage (g/g)**
54	0	0	11.41	2444.19
54	1.84	0	13.17	2183.76
44	1.35	5.07	22.35	1592.08
34	0.97	8.89	30.48	1227.12

Analysing Table 10**Erreur ! Source du renvoi introuvable.**, it becomes clear that the production rate increases with a decrease of inlet temperature, even when the amount of ICA fed into the reactor is kept constant. This is because the lower feeding temperatures allow for more heat to be removed from the reactor, but at the same time is condensing a part of the ICA, meaning that even more heat can be removed by the evaporation phenomenon. Comparing these results with those seen in case study III, it looks like dropping the feed temperature can lead to higher production rates for the same amount of liquid content, but this comes at the cost of inferior catalyst mileage. Although a bigger difference between the production rates of the two case studies could be expected, one should keep in mind that in this case study, the amount of ICA was kept constant, which is a contrast to case study II, where more ICA is being fed into the reactor to increase liquid content.

Because there are larger temperature gradients in the reactor at lower feed temperatures (see Figure 19), the molecular weight distribution of the final polymer was also studied. The results shown in Figure 20 confirm that decreasing the feed temperatures leads to a shift of the molecular weight distribution towards bigger values, as decreases in the temperature increase the molecular weight of the polymer.

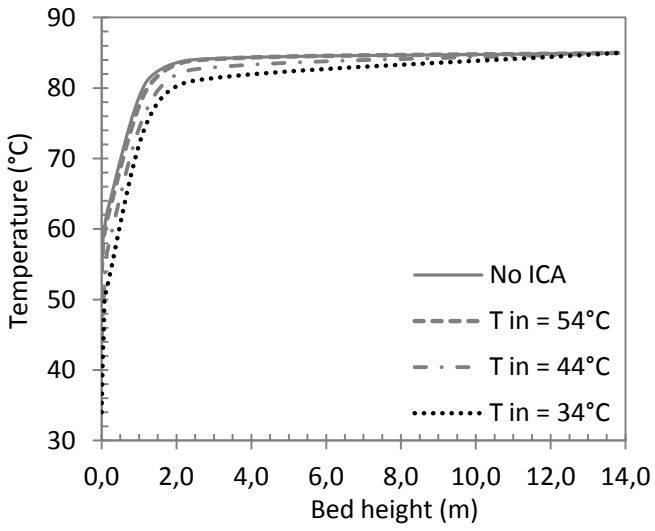

Figure 19. Effects of inlet temperature on reactor temperature profile. The simulations for no ICA had an inlet temperature of 54°C.

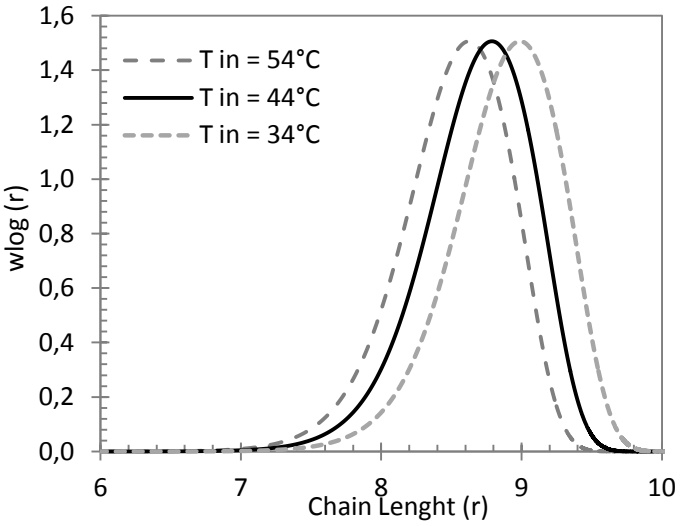

Figure 20. Effects of inlet temperature on the final product MWD.

3.2.6 Case Study V – Effects of Hydrogen

The effects of hydrogen on the reaction rate and on the molecular weight distribution (MWD) where studied for the case of n-pentane being used as an ICA. The simulations were run at a constant bulk temperature of 85°C and the partial pressure of hydrogen was varied between 0 and 3 bar.

The MWD of the recovered polymer for different hydrogen contents when no ICA is present are shown in Figure 21.

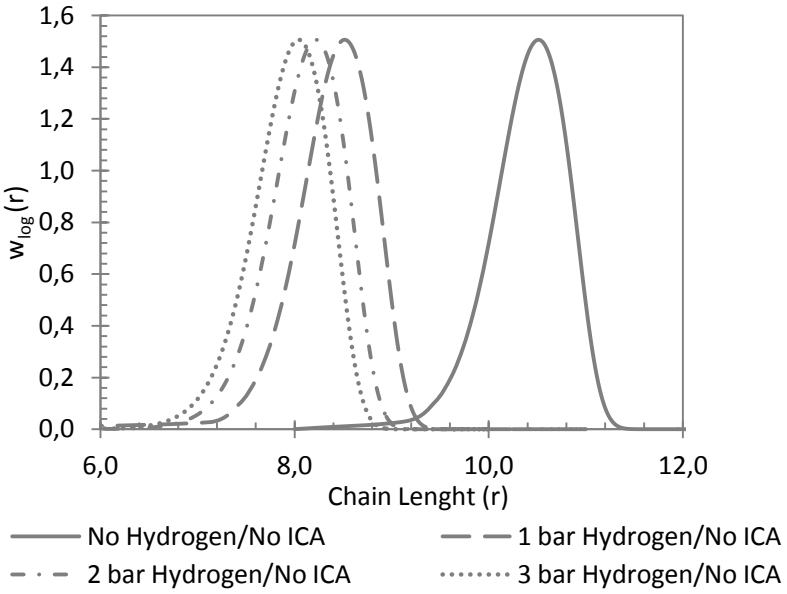

Figure 21. Log-scale mass chain length distribution for different hydrogen partial pressures in the absence of ICA. Results shown for the recovered polymer.

In this Figure, effects of hydrogen are as expected: The increase in hydrogen partial pressure shifts the molecular weight distribution to the left, decreasing the average molecular weight. In Figure 22 the effects of liquid ICA when the partial pressure of hydrogen is kept constant at 3 bar is shown. As expected the presence of more ICA shifts the molecular weight distribution to higher values due to increased ethylene concentration at the active sites. This is very much in line with the observations of Namkajorn et al. [7], who observed that adding ICA increases the average molecular weight with respect to dry mode.

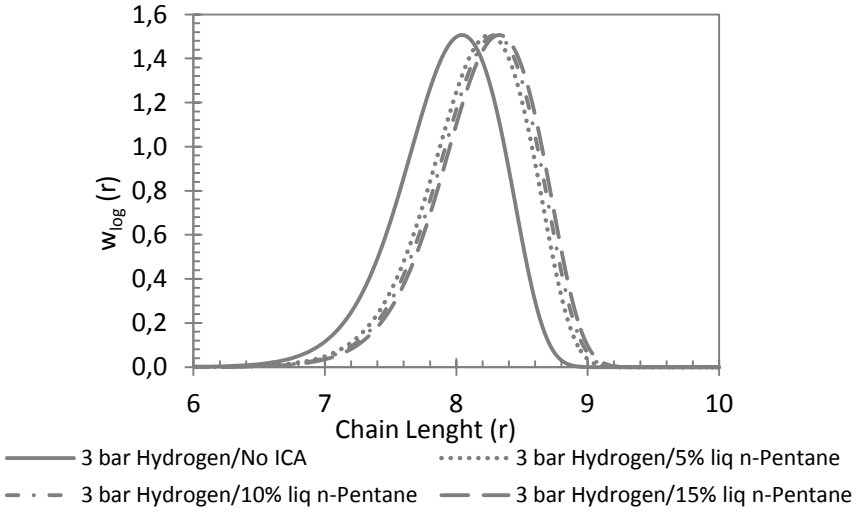

Figure 22. Log-scale mass chain length distribution for hydrogen partial pressure of 3 bar and liquid contents of n-Pentane varying from 0 to 15%. Results shown for the recovered polymer.

The effects of hydrogen in the reaction rate have also been studies in Figure 23, where the normalized rates of reaction are shown.

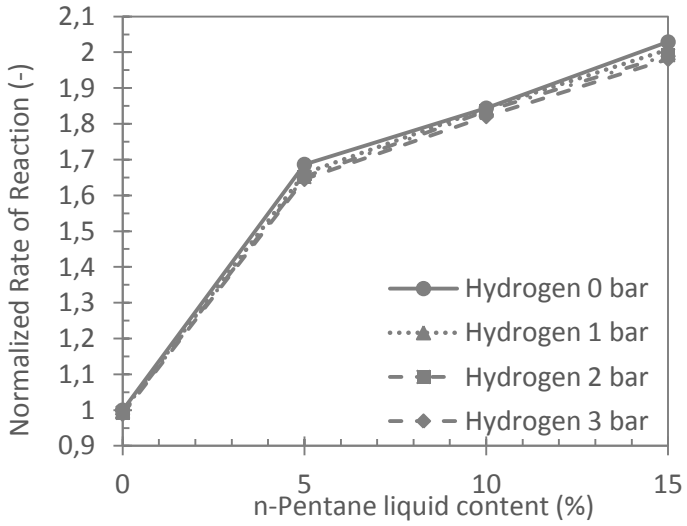

Figure 23. Normalized rate of reaction for different hydrogen and n-pentane contents.

In the figure above, the effects of hydrogen on the reaction rate are not very strong, with the curves almost overlapping. Still, a trend can be seen where the presence of hydrogen slightly

decreases the rate of reaction. This was an expected result, as the effects of hydrogen on the rate of reaction are well known and where reported by Andrade [54]. In the developed model, there were no parameters that linked the ICA and hydrogen, therefore no special correlation between the two was observed.

3.2.7 Case Study VI – Effects of droplet size

The effects of droplet size in the reactor temperature profile as well as liquid hold-up height are shown for droplets of size 50, 200, 500 and 1000 µm. Both n-pentane and n-hexane were used as ICA with 15% liquid content.

Figure 24 shows that increasing the droplet diameter increases the height of the reactor where the gas-liquid-solid phases co-exists. The results shown here are in good agreement with the projections proposed by Alizadeh *et al* [49]. Furthermore, as it is expected, it can be seen that n-hexane has a slower evaporation rate and therefore the liquid height is higher than for n-pentane, despite the fact that the number of moles of hexane is lower.

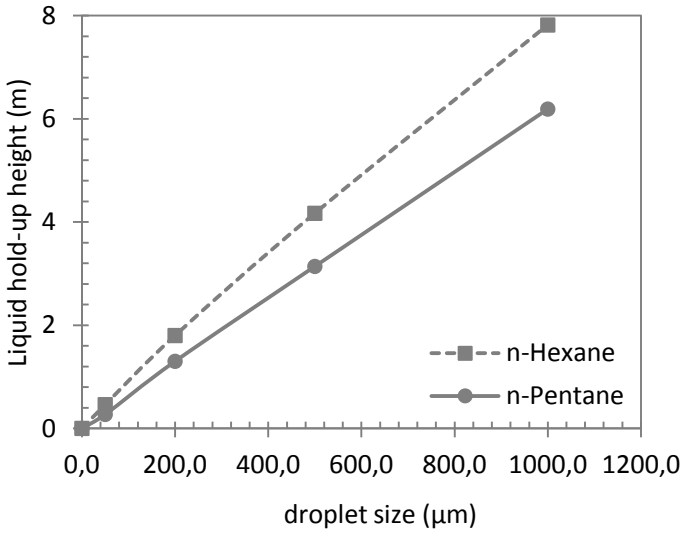

Figure 24. Liquid hold-up height in function of droplet diameter.

Figure 25 shows the effects of droplet diameter in the reactor temperature profile for the case of n-hexane. The results confirm that for droplets of 50 µm, which only occupy the bottom 0.27 m of the bed, the temperature profiles becomes sharper than the for the other two droplet sizes presented here. This is because since the liquid rapidly evaporates at the bottom of the reactor, the bed more quickly stabilizes in temperature. Comparing 200 µm and 1000 µm droplet sizes shows that the later presents the lesser sharp temperature profile of the two. This is because if the droplets are 1000 µm in diameter, they can reach up to 7.82 m in the bed, which means that the heat removal due to vaporization is more dispersed through the bed. However as the polymer is withdrawn at 1m of bed height (compartment 6), the product stream will contain large droplets of liquid which could pose a problem for downstream degassing operations. It is also interesting to see that the bottom of the reactor steeper temperature profile for 1000 µm, because less liquid is being vaporized in these compartments.

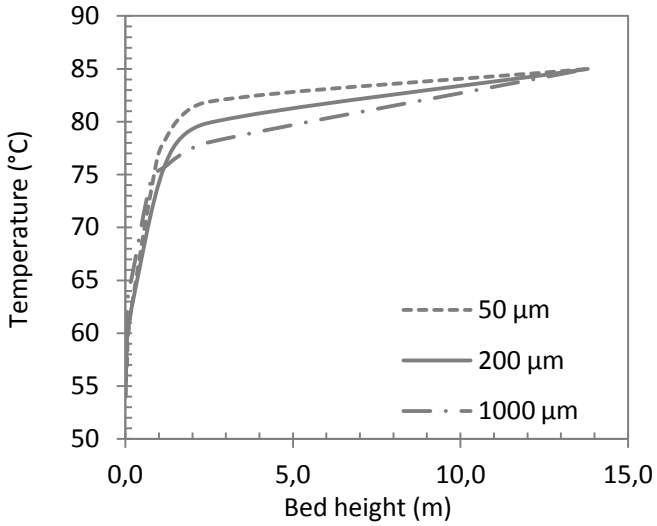

Figure 25. Reactor temperature profile with n-hexane liquid fraction of 15% for different droplet diameters of 50, 200 and 1000 µm.

3.2.8 Case Study VII – Effects of Polymer Recovery Height

The effects of the polymer recovery height on the production rate, catalyst mileage and temperature profile has been investigated at a catalyst feed rate of $6x10^{-3}$ kg/s and n-pentane liquid content of 15%. To this end three different polymer recovery heights are examined:

- 4^{th} compartment, which comprises the bed between and 0.07 and 0.1 m;
- 6^{th} compartment, which comprises the bed between 0.2 and 1.2 m
- 8^{th} (and last) compartment, which comprises the bed between 2.5 and 13.5 m.

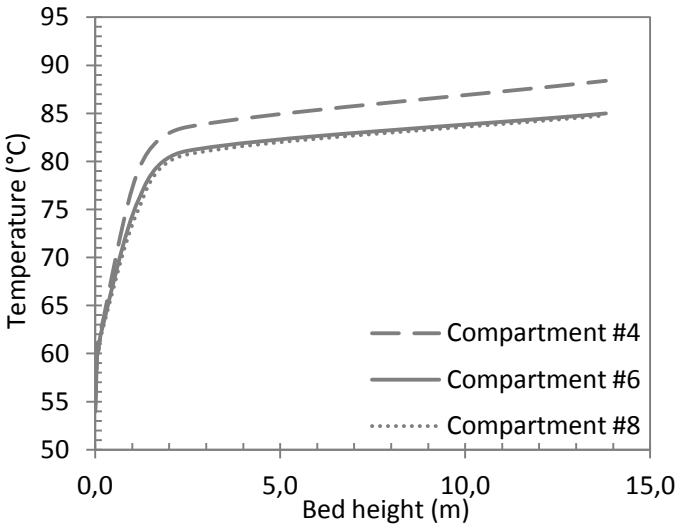

Figure 26. Temperature profiles for a different heights for polymer recovery. The catalyst feed rate is kept constant at a value of $6x10^{-3}$ kg/s. n-Pentane was used as ICA with liquid content of 15%.

Figure 26 shows that recovering polymer at the 6^{th} or 8^{th} compartment led to the same results in terms of temperature profile. The difference between the bulk temperatures at the top of the bed is only 0.22 °C. However, the simulation where the polymer is recovered at the 4^{th} compartment shows different results to those where the polymer is recovered higher in the reactor, with a

difference of 3.4 °C between the bulk temperatures at the top of the bed. This is because when the polymer is recovered from the reactor, a fraction of the liquid ICA is also recovered and thus exits the reactor before evaporating, thereby decreasing the heat removal capacity of the bed. This, combined with a constant catalyst feed flowrate, is reflected in an increase of reactor temperature. The extent of liquid loss in regard to the inlet liquid feed can be found Table 11. Since the polymerization is exothermal, the temperature rise is accompanied with a slight increase in reactor production rate and consequent increase in catalyst mileage, also shown in Table 11.

Table 11. Production rate, catalyst mileage and liquid loss for different heights for polymer recovery.

Compartment # for polymer recovery	Production Rate (ton/h)	Catalyst Mileage (g/g)	Liquid loss (%)
4	34.8	1669	2.6
6	34.0	1574	0.2
8	33.9	1568	0.0

3.2.9 Case Study VIII – Effects of Liquid Injection Height

The effects of liquid injection height in the temperature profile of the bed have been evaluated. In the previous simulations, the liquid is assumed to be injected at the bottom of the bed. In the following simulations, the liquid injection will be changed to 0.17, 1.17 and 2.47 m (respectively compartments 5, 6 and 7). Furthermore, the catalyst inlet feed rate will be kept constant at $6x10^{-3}$ kg/s and n-pentane will be used as an ICA with liquid content of 15%.

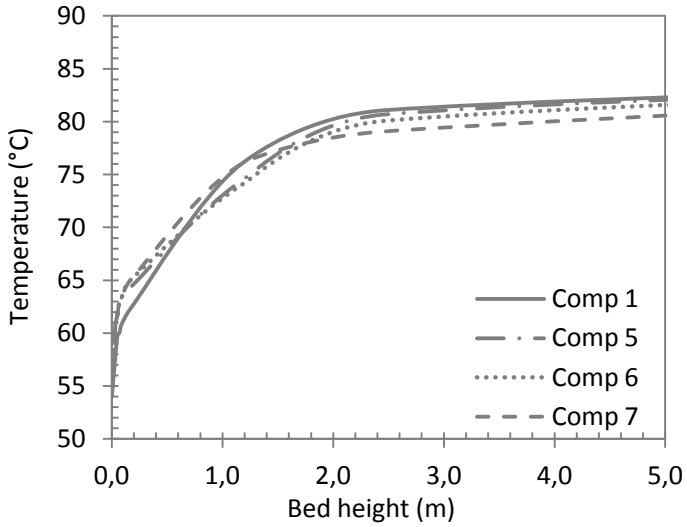

Figure 27. Temperature gradient of the bed for different liquid injection heights. The catalyst feed rate is kept constant at a value of 6x10-3 kg/s. n-Pentane was used as ICA with liquid content of 15%.

As per Figure 27, when the liquid is injected at the bottom, the temperature gradient is less steep in the lower compartments, but on the whole, the evolution of temperature in the reactor appears to cause no observable change in the production rate. This can be explained by the fact that the overall energy balance of the reactor is the same regardless of where the liquid is injected.

It is also interesting to see that the liquid height decreases when the liquid is injected higher up in the reactor, as shown in Figure 28. This is because when injecting liquid at the bottom, the temperature is lower, therefore the liquid takes longer to heat up and evaporate. If the liquid is injected higher up, the temperature surrounding the droplets is higher, effectively heating up and evaporating the liquid more quickly.

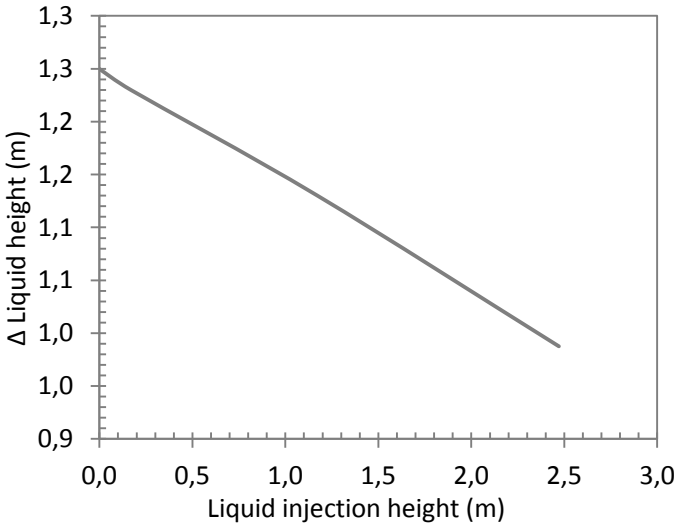

Figure 28. Liquid height for different liquid injection heights. The catalyst feed rate is kept constant at a value of $6x10^{-3}$ kg/s. n-Pentane was used as ICA with liquid content of 15%. Δ Liquid height is the difference between the height the liquid reaches in the bed and liquid injection height.

3.2.10 Case Study IX – Reactor Scale-Up/Scale-down

As the role of pilot plants units is to help understand what occurs in full scale reactors, either for the introduction of new catalysts/grades (scale-up) or for trouble-shooting an existing process (scale-down), it is useful to know if we can actually have the same temperature profiles in the reactor. The current model was used to predict the behavior in a pilot reactor, with the dimensions and other input parameters given in Table 12. This reactor is described with 7 compartments with the same height as for the full-scale model, described in Table 3, with the exception of the 7^{th} compartment, which now comprises a bed height between 1.2 and 1.7 m. The simulations were run using n-pentane as ICA and 1 bar of hydrogen.

Table 12. Inlet parameters for the pilot scale simulations.

Parameter	Unit	Value
Reactor height	m	1.7
Reactor diameter	n	0.5
Inlet gas temperature	°C	54
Inlet gas flow rate	mol/s	110
Superficial gas velocity	m/s	0.75

The obtained temperature profiles can be found in Figure 29. The results in terms of reactor production rate, catalyst mileage, liquid height and average particle size can be found in **Erreur ! Source du renvoi introuvable.**.

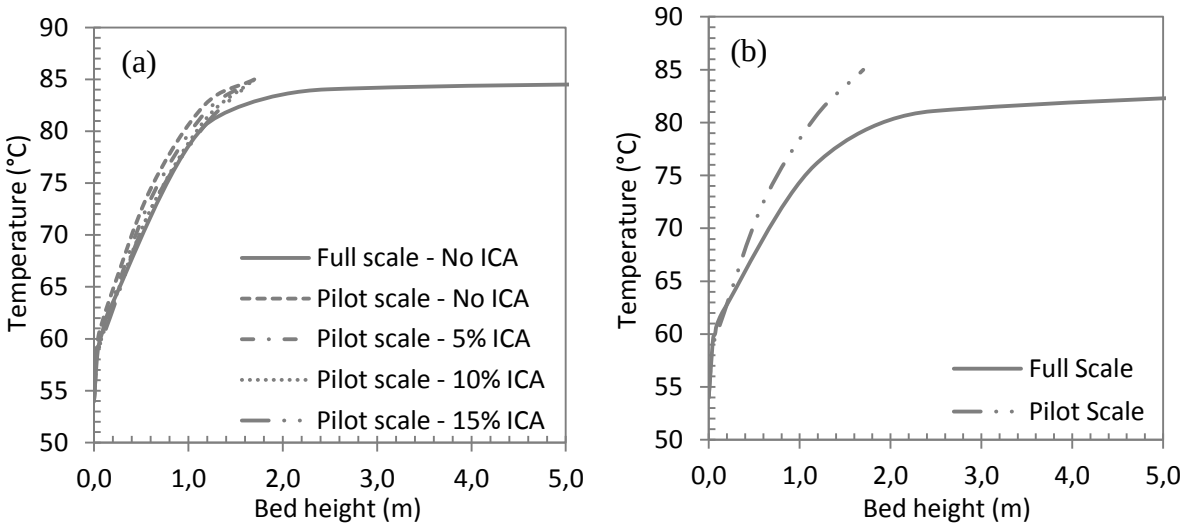

Figure 29. Temperature profiles of the bed for: (a) different liquid contents of n-pentane as ICA in a pilot plant reactor. The temperature profile for the first 5 m of the full-scale reactor are also shown for reference. (b) Comparison between full and pilot scales for 15% n-pentane liquid fraction.

Figure 29 shows that the temperature profile of the pilot scale reactor mimics that of the full-scale reactor and the effects of the ICA in the bed temperature profiles are as less pronounced that those seen on the industrial scale simulations. This might be related to the fact that in these

simulations a fixed temperature at the top of the bed has been imposed. However, in the pilot - scale the bed never reaches a stable temperature, whereas in the industrial-scale reactor 80% of the bed is above 84°C, which causes the normalized production rates and catalyst mileage to be lower for the scale down reactor, as seen in Figure 30.

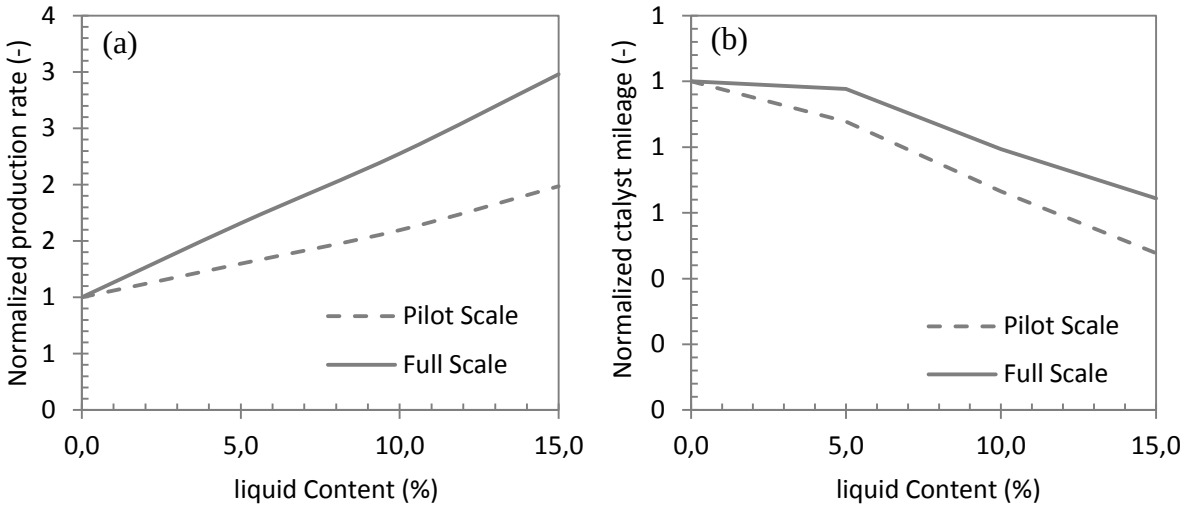

Figure 30. Pilot scale vs full scale comparison of the normalized production rate (a) and catalyst mileage (b) for different n-pentane liquid contents.

In terms of polymer properties , it is possible to see that the presence of ICA significantly decreases the average particle size (Table 13) and that the particles have a smaller size than those produced in the industrial scale reactor. This is because the residence time and the overall temperature are lower than the full-size counterpart.

Table 13. Production rate, catalyst mileage, liquid height and average particle size for different liquid contents in a pilot scale reactor.

Liquid content (%)	**Production Rate (ton/h)**	**Catalyst Mileage (g/g)**	**liquid height (m)**	**Average particle size (µm)**
0	0.020	1916	0	537
5	0.031	1820	0.27	488
10	0.038	1462	0.34	429
15	0.047	1051	0.48	397

The molecular weight distribution is also seen to shift towards bigger values in the pilot scale reactor, as seen in Figure 31. As per Figure 29, the temperature profile shows that a larger portion of the bed is at a lower temperature, meaning that a larger portion of the produced polymer is formed in the cooler region of the bed when compared to the industrial scale. Andrade [26] also investigated the temperature effects in the average molecular weight, and showed that it increased with decrease reaction temperature.

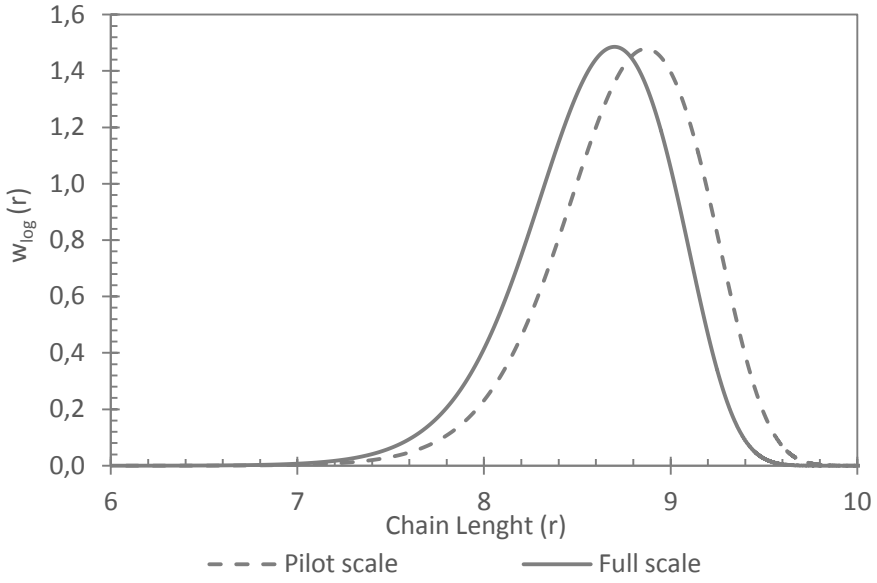

Figure 31. Molecular weight distribution for pilot and industrial scale reactors. Hydrogen partial pressure was kept at 1 bar and 10% n-pentane liquid fraction was used as an ICA.

4 Conclusions

Modelling ethylene polymerization has been the target of multiple efforts, however the thermodynamic effects that can be seen in in the presence of ICA are usually overlooked. Therefore, a multi-scale compartmentalized, one phase model has been developed and integrated with a thermodynamic model (SL-EoS), to capture the co-solubility and co-diffusion effects. Furthermore, a simplified, easier to implement model is also proposed. A novel approach to estimate compartment height was also discussed, based on the modelling objectives of this work.

The model was initially validated with data from a patent and experimental temperature profiles for condensed mode operation. The model has shown good agreement with both sources and was considered fit to describe the process for gas-phase ethylene polymerization in a fluidized bed reactor. The simplified and complete models were compared, and the simplified approach was validated for the cases of higher superficial velocity where no bed segregation is observed. For lower gas velocity, the models diverged in results. The effect of the number of compartments was also studied. Doubling the number of compartments by halving their height halved, showed that there is very little difference between the predicted PSD at the top and bottom of the bed, as well as in the temperature profiles. We therefore used the criterion of defining the bed height to limit solubility changes to 10%.

Simulations to study the impact of different ICA, reactor operating temperature, hydrogen contents and liquid droplet sizes have also been made and compared to the available experimental data. The model showed that it followed that same trends that had been experimentally observed. The effects of the liquid injection height was also evaluated, and the results show that the overall performance of the reactor remains unchanged. Furthermore, the importance of choosing operating conditions for specific polymer properties has been shown.

The model was also applied to a pilot scale reactor, and the results produced show that this might be useful tool for sale-up/down analysis. The results also show that the normalized production rate and catalyst mileage of the pilot scale reactor decrease in comparison with the industrial scale because the overall temperature gradient.

5 References

[1] R. Ferreira Alves, T. Casalini, G. Storti, and T. Mckenna, “Gas-phase Polyethylene Reactors -A Critical Review of Modelling Approaches,” *Macromol. React. Eng.*, 2021, doi: 10.1002/mren.202000059.

[2] A. E. Hamielec and J. B. P. Soares, “Polymerization reaction engineering - Metallocene catalysts,” *Progress in Polymer Science (Oxford)*, vol. 21, no. 4. Elsevier Ltd, pp. 651–706, 1996, doi: 10.1016/0079-6700(96)00001-9.

[3] M. R. Abbasi, A. Shamiri, and M. A. Hussain, “A review on modeling and control of olefin polymerization in fluidized-bed reactors,” *Reviews in Chemical Engineering*, vol. 35, no. 3. De Gruyter, pp. 311–333, Apr. 01, 2019, doi: 10.1515/revce-2017-0040.

[4] Y. P. Zhu, G. Q. Chen, and Z. H. Luo, “Particle behavior in FBRs: A comparison of the PBM-CFD, multi-scale CFD simulation of gas-solid catalytic propylene polymerization,” *Macromol. React. Eng.*, vol. 8, no. 9, pp. 609–621, Sep. 2014, doi: 10.1002/mren.201300196.

[5] M. Namkajorn, A. Alizadeh, E. Somsook, and T. F. L. McKenna, “Condensed Mode Cooling for Ethylene Polymerisation : The Influence of Inert Condensing Agent on the Polymerisation Rate,” *Macromol. Chem. Phys.*, vol. 215, no. 9, pp. 873–878, 2014.

[6] A. Alizadeh, M. Namkajorn, E. Somsook, and T. F. L. McKenna, “Condensed Mode Cooling for Ethylene Polymerization: Part I. The Effect of Different Induced Condensing Agents on Polymerization Rate,” *Macromol. Chem. Phys.*, vol. 216, no. 8, pp. 903–913, 2015.

[7] A. Alizadeh, M. Namkajorn, E. Somsook, and T. F. L. McKenna, “Condensed Mode Cooling for Ethylene Polymerization: Part II. From Cosolubility to Comonomer and Hydrogen Effects,” *Macromol. Chem. Phys.*, vol. 216, no. 9, pp. 985–995, 2015.

[8] A. Wonders, G. E. Moore, R. R. Ford, F. D. Daily, K. A. Dooley, and J. J. Garcia,

"Suppression of Fines in Fluid Bed Polyethylene Process," Patent US 5969061, 1999.

[9] V. Kanellopoulos, D. Mouratides, E. Tsiliopoulou, and C. Kiparissides, "An Experimental and Theoretical Investigation into the Diffusion of Olefins in Semi-Crystalline Polymers: The Influence of Swelling in Polymer-Penetrant Systems," *Macromol. React. Eng.*, vol. 1, no. 1, pp. 106–118, 2007.

[10] R. F. Alves and T. F. L. McKenna, "Estimation of diffusion coefficients for multiple penetrant/polyolefin systems based on sorption data," *Chem. Eng. J.*, vol. 383, 2019, doi: 10.1016/j.cej.2019.123114.

[11] F. N. Andrade, R. Fulchiron, F. Collas, and T. F. L. McKenna, "Condensed Mode Cooling for Ethylene Polymerization: Part V—Reduction of the Crystallization Rate of HDPE in the Presence of Induced Condensing Agents," *Macromol. Chem. Phys.*, vol. 220, no. 9, p. 1800563, May 2019, doi: 10.1002/macp.201800563.

[12] R. E. Pequeno, R. O. Hagerty, and B. Savatsky, "Bulk Density Promoting Agents in a Gas-phase Polymerazation Process to Achieve a Bulk Particle Density," US 7754834 B2, 2010.

[13] T. Xie, K. B. McAuley, J. C. C. Hsu, and D. W. Bacon., "Gas phase ethylene polymerization: Production processes, polymer properties, and reactor modeling," *Ind. Eng. Chem. Res.*, vol. 33, no. 3, pp. 449–479, 1994.

[14] C. Kiparissides, "Polymerization reactor modeling: A review of recent developments and future directions," *Chem. Eng. Sci.*, vol. 51, no. 10, pp. 1637–1659, 1996, doi: 10.1016/0009-2509(96)00024-3.

[15] A. Mirzaei, A. Kiashemshaki, and M. Emanmi, "Fluidized Bed Polyethylene Reactor Modeling in Condensed Mode Operation," *Macromol. Symp.*, vol. 259, no. 1, pp. 135–144, 2007.

[16] Y. Zhou, J. Wang, Y. Yang, and W. Wu, "Modeling of the Temperature Profile in an

Ethylene Polymerization Fluidized-Bed Reactor in Condensed-Mode Operation," *Ind. Eng. Chem. Res.*, vol. 52, no. 12, p. 4455−4464, 2013.

[17] X. Fan *et al.*, "Thermal-Stability Analysis of Ethylene-Polymerization Fluidized-Bed Reactors under Condensed-Mode Operation through a TPM-PBM Integrated Model," *Ind. Eng. Chem. Res.*, vol. 58, no. 22, pp. 9486–9499, 2019, doi: 10.1021/acs.iecr.9b00071.

[18] R. Alves, M. A. Bashir, and T. F. L. McKenna, "Modeling Condensed Mode Cooling for Ethylene Polymerization: Part II. Impact of Induced Condensing Agents on Ethylene Polymerization in an FBR Operating in Super-Dry Mode," *Ind. Eng. Chem. Res.*, vol. 56, no. 46, pp. 13582–13593, 2017, doi: 10.1021/acs.iecr.7b02963.

[19] A. Bragança, A. Morschbacker, E. Rubbo, C. Miro, T. Barlem, and A. Mukherjee, "Process for the gas phase polymerization and copolymerization of olefin monomers," US 6864332 B2, 2005.

[20] M. Alizadeh, N. Mostoufi, S. Pourmahdian, and R. Sotudeh-Gharebagh, "Modeling of fluidized bed reactor of ethylene polymerization," *Chem. Eng. J.*, vol. 97, no. 1, pp. 27–35, 2004, doi: 10.1016/S1385-8947(03)00133-5.

[21] O. Ashrafi, H. Nazari-Pouya, N. Mostoufi, and R. Sotudeh-Gharebagh, "Particle size distribution in gas-phase polyethylene reactors," *Adv. Powder Technol.*, vol. 19, no. 4, pp. 321–334, 2008, doi: 10.1163/156855208X314967.

[22] H. Hatzantonis, A. Goulas, and C. Kiparissides, "A comprehensive model for the prediction of particle-size distribution in catalyzed olefin polymerization fluidized-bed reactors," *Chem. Eng. Sci.*, vol. 53, no. 18, pp. 3251–3267, 1998, doi: 10.1016/S0009-2509(98)00122-5.

[23] G. Dompazis, A. Roussos, V. Kanellopoulos, and C. Kiparissides, "Dynamic evolution of the particle size distribution in multistage olefin polymerization reactors," *Comput. Aided*

Chem. Eng., vol. 20, no. C, pp. 427–432, 2005, doi: 10.1016/S1570-7946(05)80193-2.

[24] J. B. P. Soares and T. F. L. McKenna, *Polyolefin Reaction Engineering*. Wiley-VCH, 2012.

[25] A. R. Albunia, F. Prades, and D. Jeremic, *Multimodal polymers with supported catalysts: Design and production*. Springer International Publishing, 2019.

[26] S. K. GUPTA, "Low density polyethylene (LDPE) polymerization — A review," *Curr. Sci.*, vol. 56, no. 19, pp. 979–984, 1987.

[27] J. B. P. Soares, "Mathematical modelling of the microstructure of polyolefins made by coordination polymerization: A review," *Chem. Eng. Sci.*, vol. 56, no. 13, pp. 4131–4153, 2001, doi: 10.1016/S0009-2509(01)00083-5.

[28] A. Alizadeh, "Study of Sorption, Heat and Mass Transfer During Condensed Mode Operation of Gas Phase Ethylene Polymerization on Supported Catalyst," Queen's University, 2014.

[29] A. Alizadeh, J. Chmelař, F. Sharif, M. Ebrahimi, J. Kosek, and T. F. L. McKenna, "Modeling Condensed Mode Operation for Ethylene Polymerization: Part I. Thermodynamics of Sorption," *Ind. Eng. Chem. Res.*, vol. 56, no. 5, pp. 1168–1185, Feb. 2017, doi: 10.1021/acs.iecr.6b04288.

[30] W. Yao, X. Hu, and Y. Yang, "Modeling solubility of gases in semicrystalline polyethylene," *J. Appl. Polym. Sci.*, vol. 103, no. 3, pp. 1737–1744, Feb. 2007, doi: 10.1002/app.24969.

[31] M. A. Bashir, V. Monteil, V. Kanellopoulos, M. A.-H. Ali, and T. F. L. McKenna, "Partial Molar Volumes and Thermal Expansion Coefficients as an Explanation for Co-Solvent Effect of Penetrants in Multicomponent Polymer Mixtures," *Macromol. Chem. Phys.*, vol. 216, no. 21, pp. 2129–2140, Nov. 2015, doi: 10.1002/macp.201500170.

[32] I. C. Sanchez and R. H. Lacombe, “An elementary equation of state for polymer liquids,” *J. Polym. Sci. Polym. Lett. Ed.*, vol. 15, no. 2, pp. 71–75, Feb. 1977, doi: 10.1002/pol.1977.130150202.

[33] I. C. Sanchez and R. H. Lacombe, “An elementary molecular theory of classical fluids. Pure fluids,” *J. Phys. Chem.*, vol. 80, no. 21, pp. 2352–2362, Oct. 1977, doi: 10.1021/j100562a008.

[34] A. Ben Mrad, N. Sheibat-Othman, J. Hill, M. Bartke, and T. F. L. McKenna, “A novel approach for the estimation of the Sanchez-Lacombe interaction parameters for the solubility of ternary polyolefins systems,” *Chem. Eng. J.*, p. 127778, Nov. 2020, doi: 10.1016/j.cej.2020.127778.

[35] M. A. Bashir, M. Al-haj Ali, V. Kanellopoulos, and J. Seppälä, “Modelling of multicomponent olefins solubility in polyolefins using Sanchez-Lacombe equation of state,” *Fluid Phase Equilib.*, vol. 358, pp. 83–90, 2013, doi: 10.1016/j.fluid.2013.08.009.

[36] S. Floyd, K. Y. Choi, T. W. Taylor, and W. H. Ray, “Polymerization of Olefins through Heterogeneous Catalysis III. Polymer Particle Modelling with an Analysis of Intraparticle Heat and Mass Transfer Effects,” *J. Appl. Polym. Sci*, vol. 32, no. 1, pp. 2935–2960, 1986.

[37] V. Kanellopoulos, G. Dompazis, B. Gustafsson, and C. Kiparissides, “Comprehensive analysis of single-particle growth in heterogeneous olefin polymerization: The random-pore polymeric flow model,” *Ind. Eng. Chem. Res.*, vol. 43, no. 17, pp. 5166–5180, 2004, doi: 10.1021/ie030810u.

[38] R. B. (Robert B. Bird, W. E. Stewart, and E. N. Lightfoot, *Transport phenomena*. J. Wiley, 2007.

[39] A. Alizadeh, F. Sharif, M. Ebrahimi, and T. F. L. McKenna, “Modeling Condensed Mode Operation for Ethylene Polymerization: Part III. Mass and Heat Transfer,” *Ind. Eng. Chem.*

Res., vol. 57, no. 18, pp. 6097–6114, May 2018, doi: 10.1021/acs.iecr.8b00330.

[40] V. Kanellopoulos, E. Tsiliopoulou, G. Dompazis, V. Touloupides, and C. Kiparissides, "Evaluation of the internal particle morphology in catalytic gas-phase olefin polymerization reactors," *Ind. Eng. Chem. Res.*, vol. 46, no. 7, pp. 1928–1937, 2007, doi: 10.1021/ie060721s.

[41] S. Floyd, K. Y. Choi, T. W. Taylor, and W. H. Ray, "Polymerization of Olefins Through Heteregeneous Catalysis IV. Modeling of Heat and Mass Transfer Resistance in the Polymer Particle Boundary Layer," *J. Appl. Polym. Sci*, vol. 31, no. 7, pp. 2231–2265, 1986.

[42] K. Y. Choi, X. Zhao, and S. Tang, "Population balance modeling for a continuous gas phase olefin polymerization reactor," *J. Appl. Polym. Sci.*, vol. 53, no. 12, pp. 1589–1597, Sep. 1994, doi: 10.1002/app.1994.070531205.

[43] D. Kunii and O. Levenspiel, *Fluidization Engineering*, 2nd Editio. Butterworth-Heinemann, 1991.

[44] D. Geldart, J. Cullinan, S. Georghiades, D. Gilvray, and D. J. Pope, "EFFECT OF FINES ON ENTRAINMENT FROM GAS FLUIDISED BEDS.," *Trans. Inst. Chem. Eng.*, vol. 57, no. 4, pp. 269–275, 1979.

[45] N. Selçuk, O. Oymak, and E. Değirmenci, "Basic requirement for modelling fluidized beds: Fast computation of particle size distributions (PSDs)," *Powder Technology*, vol. 87, no. 3. Elsevier, pp. 269–271, Jun. 01, 1996, doi: 10.1016/0032-5910(96)03112-9.

[46] J.-C. Chinh, M. C. H. Filippelli, D. Newton, and M. B. Power, "POLYMERIZATION PROCESS 75," US Patent 6001938, 1999.

[47] T. F. L. McKenna, "Condensed Mode Cooling of Ethylene Polymerization in Fluidized Bed Reactors," *Macromolecular Reaction Engineering*, vol. 13, no. 2. p. 1800026, Apr.

15, 2019, doi: 10.1002/mren.201800026.

[48] S. J. Rhee and L. L. Simpson, “Fluidized Bed Polymerization Reactors,” US 4933149, 1990.

[49] A. Alizadeh and T. F. L. McKenna, “Condensed mode cooling in ethylene polymerisation: droplet evaporation,” *Macromol. Symp.*, vol. 333, no. 1, pp. 242–247, Nov. 2013, doi: 10.1002/masy.201300092.

[50] A. Leach, G. Chaplin, C. Briens, and F. Berruti, “Comparison of the performance of liquid-gas injection nozzles in a gas-solid fluidized bed,” *Chem. Eng. Process. Process Intensif.*, vol. 48, no. 3, pp. 780–788, Mar. 2009, doi: 10.1016/j.cep.2008.10.002.

[51] R. P. Utikar, Y. M. Harshe, A. Mehra, and V. V. Ranade, “Modeling of a fluidized bed propylene polymerization reactor operated in condensed mode,” *J. Appl. Polym. Sci.*, vol. 108, no. 4, pp. 2067–2076, May 2008, doi: 10.1002/app.27748.

[52] S. Mawson, J. F. Szul, M. G. Goode, and C. C. Williams, “Polymerization Process,” US 6489408, 2002.

[53] A. Alizadeh and T. F. L. McKenna, “Condensed Mode Cooling for Ethylene Polymerization: The Influence of the Heat of Sorption,” *Macromol. React. Eng.*, vol. 8, no. 5, pp. 419–433, May 2014, doi: 10.1002/mren.201300165.

[54] F. N. Andrade, “Effect of condensable materials during the gas phase polymerization of ethylene on supported catalysts,” Université Lyon 1, 2019.